Spin-Lattice Relaxation of Coupled Metal-Radical Spin-Dimers in Proteins: Application to Fe^{2+}-Cofactor (Q_A^-, Q_B^-, ϕ^-) Dimers in Reaction Centers from Photosynthetic Bacteria

Rafael Calvo,*† Roger A. Isaacson,† Edward C. Abresch,† Melvin Y. Okamura,† and George Feher†

*Departamento de Física, Facultad de Bioquímica y Ciencias Biológicas, Universidad Nacional del Litoral and INTEC (CONICET-UNL), 3000 Santa Fe, Argentina, and †Department of Physics, University of California, San Diego, La Jolla, California 92093-0319 USA

ABSTRACT The spin-lattice relaxation times (T_1) for the reduced quinone acceptors Q_A^- and Q_B^-, and the intermediate pheophytin acceptor ϕ^-, were measured in native photosynthetic reaction centers (RC) containing a high spin Fe^{2+} ($S = 2$) and in RCs in which Fe^{2+} was replaced by diamagnetic Zn^{2+}. From these data, the contribution of the Fe^{2+} to the spin-lattice relaxation of the cofactors was determined. To relate the spin-lattice relaxation rate to the spin-spin interaction between the Fe^{2+} and the cofactors, we developed a spin-dimer model that takes into account the zero field splitting and the rhombicity of the Fe^{2+} ion. The relaxation mechanism of the spin-dimer involves a two-phonon process that couples the fast relaxing Fe^{2+} spin to the cofactor spin. The process is analogous to the one proposed by R. Orbach (*Proc. R. Soc. A. (Lond.).* 264:458–484) for rare earth ions. The spin-spin interactions are, in general, composed of exchange and dipolar contributions. For the spin dimers studied in this work the exchange interaction, J_o, is predominant. The values of J_o for $Q_A^-Fe^{2+}$, $Q_B^-Fe^{2+}$, and ϕ^-Fe^{2+} were determined to be (in kelvin) -0.58, -0.92, and -1.3×10^{-3}, respectively. The $|J_o|$ of the various cofactors (obtained in this work and those of others) could be fitted with the relation $\exp(-\beta_J d)$, where d is the distance between cofactor spins and β_J had a value of (0.66-0.86) $Å^{-1}$. The relation between J_o and the matrix element $|V_{ij}|^2$ involved in electron transfer rates is discussed.

INTRODUCTION

Several studies of the electron spin-lattice relaxation times (T_1) of radicals in metalloproteins have been reported (Bowman et al., 1979; Norris et al., 1980; Calvo et al., 1982; Sahlin et al., 1987; Styring and Rutherford, 1988; Innes and Brudvig, 1989; Hirsh et al., 1992a, b, 1993; Koulougliotis et al., 1995, 1997; Galli et al., 1995, 1996; Deligiannakis and Rutherford, 1996; Waldeck et al., 1997; Hung et al., 2000; Telser et al., 2000; Bar et al., 2001). T_1 is the time needed to reach thermodynamic equilibrium between the spin system and the molecular (lattice) vibrations. T_1 is shortened when the radical interact with the spin of a fast relaxing paramagnetic ion in its vicinity. Using an appropriate model, one can evaluate the spin-spin interaction from the experimentally determined value of the spin-lattice relaxation time. The spin-spin interaction contains information about the electronic and spatial structure of the spin-dimer, which in many cases are important in understanding electron transfer processes.

The spin-spin interactions between the metal ion and the radicals contains exchange and dipole-dipole contributions. Exchange interactions are related to two-electron exchange integrals and to overlap integrals of the magnetic orbitals that provide the superexchange path (Anderson, 1959). Their evaluation requires a detailed knowledge of the electronic structure of the molecular bridge connecting the spins. This has been done only for unpaired spins connected by simple chemical paths (Kahn, 1993). Analyses based on experimental values for a large number of compounds indicate that the exchange contribution J_o dominates over the dipolar contribution for short distances R between the spins ($R < \lambda$), while dipolar contributions dominate for longer distances ($R > \lambda$) (Coffman and Buettner, 1979; Hoffmann et al., 1994). The value of λ has been determined empirically and has changed with time as the experimental database expanded. The most recent value of λ proposed by Hoffmann et al. (1994) is ~35 Å. However, it should be kept in mind that the value of λ depends on the electronic structure of the pathway and, therefore, will vary for different classes of compounds. The RC, which has been optimized for efficient electron transfer, may not necessarily be representative of an average protein.

Relatively little is known about exchange interactions between unpaired spins within a protein. The connecting paths involve covalent and non-covalent bonds, H-bonds, and space jumps. Exchange interactions have been related to electron transfer rates when the unpaired spins are components of an electron transfer reaction (Hopfield, 1974; Okamura et al., 1979a, b; DeVault, 1984; Hendrickson, 1985; Michel-Beyerle et al., 1988; Calvo et al., 2000). Thus, a determination of the exchange interaction can contribute to the understanding of the electron transfer processes.

Dipolar interactions are related to the distance between the interacting spins and to the orientation of the applied magnetic field with respect to the molecular axes (Slichter, 1990). Thus, dipolar interactions provide direct information about the three-dimensional molecular structure (e.g., Calvo

Submitted April 12, 2002, and accepted for publication July 12, 2002.

Address reprint requests to George Feher, Physics Department, University of California, San Diego, 9500 Gilman Dr., La Jolla, CA 92093-0319. Tel.: 858-534-4388; Fax: 858-822-0007; E-mail: gfeher@physics.ucsd.edu.

0006-3495/02/11/2440/17 $2.00

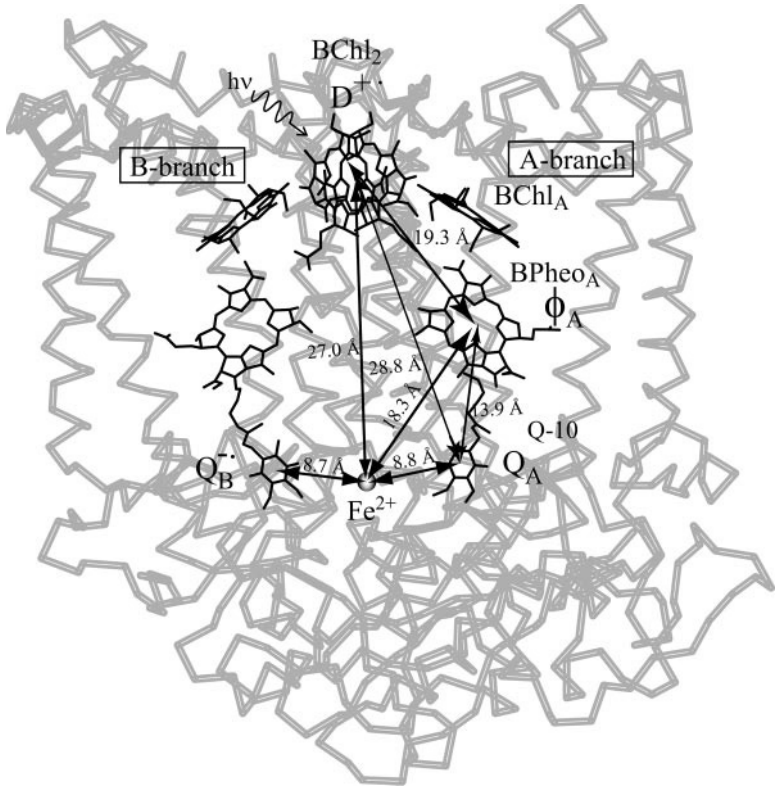

FIGURE 1 Structure of the cofactors in the photosynthetic reaction center from *Rb. sphaeroides*, with the protein polypeptide chains in the background (Stowell et al., 1997). Distances are determined between the Fe^{2+} ion and the centers of the rings of ϕ^-, Q_A^-, and Q_B^-. For D^+, the distance was taken from the center of the line connecting the two Mg^{2+} atoms.

et al., 2000). This provides important information for proteins whose x-ray structure has not been determined.

Spin-spin interactions often modify the electron paramagnetic resonance (EPR) signal. Thus, EPR spectroscopy may be used in these cases to evaluate spin-spin interactions (Bencini and Gatteschi, 1990). [In this paper we use Kelvin as the energy (E) units (*i.e.*, E/k_B, where k_B is the Boltzmann constant). The conversion factors are: 1 K = 1.3805×10^{-23} Joule = 8.617×10^{-5} eV = 0.6950 cm^{-1} = 2.0837×10^{10} Hz = 7443.7 Gauss (for $g = 2$)]. In some cases, in particular when the interaction is very small, no observable effect on the EPR spectrum is observed. In these cases, the spin-spin interaction may express itself in a change of the spin-lattice relaxation time. This situation is analyzed in detail in this paper. Thus, spin-lattice relaxation measurements complement standard EPR spectroscopy for the characterization of spin-spin interactions.

The system studied in this work is the reaction center (RC) of the photosynthetic bacterium *Rhodobacter sphaeroides*. The RC is a membrane-bound pigment protein complex that performs the primary photochemistry by coupling light-induced electron transfer to vectorial proton transfer across the bacterial membrane (reviewed by Cramer and Knaff (1991)). Light-induced electron transfer proceeds from a primary donor (a bacteriochlorophyll dimer, D), through a series of electron donor and acceptor molecules (a bacteriopheophytin ϕ and a quinone molecule Q_A) to a loosely bound secondary quinone (Q_B), which serves as a mobile electron and proton carrier. There is an Fe^{2+} ion located between Q_A and Q_B whose properties have been studied by several techniques (reviewed by Feher and Okamura, 1999).

The electronic structures of the ionized pigments (Q_A^-, Q_B^-, ϕ^-, and D^+) have been studied in detail by EPR and ENDOR (reviewed by Feher (1992) and Lubitz and Feher (1999)). The x-ray structure of the RC of *Rb. sphaeroides* is well known (Allen et al., 1986, 1987a, b, 1988; Chang et al., 1986; Yeates et al., 1987, 1988; Ermler et al., 1994; Stowell et al., 1997; Abresch et al., 1999). Fig. 1 displays the structure of the cofactors and the Fe^{2+} ion within the RC when Q_B^- is reduced (Stowell et al., 1997). The distances between the Fe^{2+} ion and the cofactors, and between some pairs of cofactors, are indicated. For Q_A^-, Q_B^-, and ϕ^- they were taken between the centers of the cofactor rings. For D^+, the distance was taken from the midpoint between the Mg^{2+} ions of the two bacteriochlorophyll molecules.

The temperature dependence of the spin-lattice relaxation time of Q_A^- in *Rb. sphaeroides* had been previously studied by us (Calvo et al., 1982). In that work we showed that the relaxation times, which were of the order of microseconds in the temperature range between 1.3 and 4.2 K, are a consequence of the coupling of the Q_A^- spin with the fast relaxing Fe^{2+} spin. The data were well fitted by a two-step process allowing simultaneous transitions of the iron and quinone spins. The analysis gave a zero field splitting between the two lowest levels of the Fe^{2+} spin, in good agreement with the value obtained from magnetic susceptibility and EPR data

(Butler et al., 1980, 1984). In this work we extend the previous investigation to measure the spin-lattice relaxation times of three cofactor radicals (Q_A^-, Q_B^-, and ϕ^-) within the photosynthetic reaction center as a function of temperature (T), in the range between 1.4 and 4.2 K (in this temperature range the contribution of higher excited states of the Fe^{2+} can be neglected). The contribution of the Fe^{2+} to the relaxation times of the cofactor spins was obtained by comparing T_1 in native RCs, with T_1 in RCs in which Fe^{2+} was replaced by diamagnetic Zn^{2+} (Debus et al., 1986; Utschig et al., 1997). The results are analyzed using a theoretical model, which explicitly takes into account the crystal field splitting and rhombicity of the Fe^{2+}. This is an important point because the more plentiful phonons at the energy of the zero field splitting, which is considerably larger than the Zeeman energy, are more effective in the two-phonon relaxation process of the cofactor spins. The relaxation process for the cofactors is similar to that proposed by Orbach (1961) for rare earth ions having low excited energy states, and to that observed for Fe^{3+} in heme proteins (Scholes et al., 1971; Herrick and Stapleton, 1976). Other authors addressing the problem of spin-lattice relaxation of cofactors in the RC (Bowman et al., 1979; Norris et al., 1980; Hirsh and Brudvig, 1993; reviewed by Lakshmi and Brudvig, 2000) have neglected to take the crystal field splitting and rhombicity into account, which can result in an error in the predicted value of T_1 of several orders of magnitude. These authors follow essentially the theoretical treatments of Bloembergen et al. (1948, 1949, 1961) and Abragam (1955, 1961), which were developed for the relaxation of nuclear spins. These theories are applicable to electron-electron interaction only when the fast relaxing magnetic ion does not have a crystal field splitting (*e.g.*, a low-spin Fe^{3+} ion).

There are two different aspects of the relaxation problem. One deals with the evaluation of the spin-spin interaction from measured relaxation times. This is accomplished by using the spin-dimer model developed in this work. The other aspect deals with the determination of the source of the interaction (exchange or dipolar) and its relation to the structure (*e.g.*, distances between cofactors) which for the RC in *Rb. sphaeroides* is well known. Our analysis of the data provides a check of the validity of our model so that it can be used with confidence to investigate less well-characterized metaloproteins. An analysis of the distance dependence of the exchange interaction between unpaired spins within the RC can shed light on electron transfer matrix elements. Preliminary results of this work have been reported (Calvo et al., 1982, 1999).

MATERIALS AND METHODS

Preparation of reaction center samples

Reaction centers were isolated from *Rb. sphaeroides* R26 and purified as described previously (Isaacson et al., 1995). Zinc-containing RCs were obtained by replacing the native iron with zinc using the procedure developed by Debus et al. (1986) and modified by Utschig et al. (1997). The detergent LDAO in the buffer was exchanged with maltoside by binding the RCs to a DEAE column, washing with 10 mM Tris-Cl, 0.04% *n*-dodecyl-β-D-maltoside, eluting with 0.2 M NaCl in the same buffer, and dialyzing against 10 mM Tris-Cl pH 8, 0.04% *n*-dodecyl-β-D-maltoside.

The value of T_1 was found to depend on the amount of oxygen in solution. Consequently, great care was taken to deoxygenate the solution by adding, under an argon atmosphere, 0.9% glucose, 7.5 units/ml glucose oxidase, and 7.5 units/ml catalase to the buffer. Furthermore, the freezing protocol and buffer composition, which could affect T_1, were kept the same for the Fe^{2+} and Zn^{2+} RCs. This was particularly important for the ϕ^- samples in which the values of T_1 of ϕ^-Fe^{2+} and ϕ^-Zn^{2+} were of the same order of magnitude.

The free radical states of the cofactors were prepared as follows.

Q_A^-

The Q_A^- RC samples were diluted to an optical absorbance $A_{800}^{1\ cm} = 20$ in the deoxygenated buffer described above to which 100 μM stigmatellin was added to displace Q_B. Thirty-five microliters of the sample was placed in a 2 mm I.D. quartz tube filled with argon and equilibrated for 30 min. After adding 1.2 mM 3,6-diaminodurene (Aldrich, Milwaukee, WI) to reduce D^+, the sample was given a 1 μs saturating laser flash (500 mJ) at 590 nm from a dye laser (PhaseR Corp., New Durhan, NH) to form $D\phi Q_A^-$, and immediately plunged into liquid nitrogen.

Q_B^-

For the Q_B^- sample, a five times excess of ubiquinone (Sigma, St. Louis, Mo)/RC in ethanol solution was dried onto a vial. RCs were added to the vial and stirred for ~4 h at 23°C, resulting in a Q_B occupancy of ≥80%. Q_B^- was then made in the same manner as Q_A^-, but without the addition of stigmatellin.

ϕ^-

The RCs used to make ϕ^-Fe^{2+} and ϕ^-Zn^{2+} were treated with the same metal replacement procedure, *i.e.*, to metal-depleted RCs either Fe^{2+} or Zn^{2+} was added (Debus et al., 1986; Utschig et al., 1997); ϕ^- was made as described by Okamura et al. (1979b) with the following modifications. RCs were diluted into buffer containing 50 mM Tris pH 8, 0.1% Triton X-100, 0.2 mM cytochrome c_2, 0.9% glucose, 7.5 units/ml glucose oxidase, and 7.5 units/ml catalase to a final concentration of $A_{800}^{1\ cm} = 20$. A 35 μl aliquot of the sample was placed in a 2 mm I.D. quartz tube filled with argon and equilibrated for 30 min; ~100 mM sodium dithionite and 100 mM Tris base was added and ϕ^- was generated by illuminating with a tungsten light source ($P = 0.4$ W/cm^2) after being filtered with 2 cm of water and a 660 nm cutoff filter (Corning 2-64). The accumulation of ϕ^- was monitored by the optical absorption at 645 nm on a Cary 50 spectrophotometer (Varian, Inc., Palo Alto, CA). When the absorbance at 645 nm reached a plateau after 1-2 min, indicating a maximal concentration of ϕ^-, the sample was plunged into liquid nitrogen.

EPR and relaxation time measurements

Spin-lattice relaxation measurements were performed at 9 GHz by measuring the recovery of the EPR signal after a saturating microwave pulse, using a superheterodyne EPR spectrometer of local design (Feher, 1957; McElroy et al., 1974). To switch between saturating and measuring microwave power levels, a HP8735A Pin diode modulator (Hewlett-Packard, Palo Alto, CA) was used. The modulator was bypassed by two directional couplers having a total attenuation of 30 db. Thus, when the modulator was in the off state (~50 db attenuation) the level of the measuring microwave power was governed by the by-pass arm, and not by the pin diode

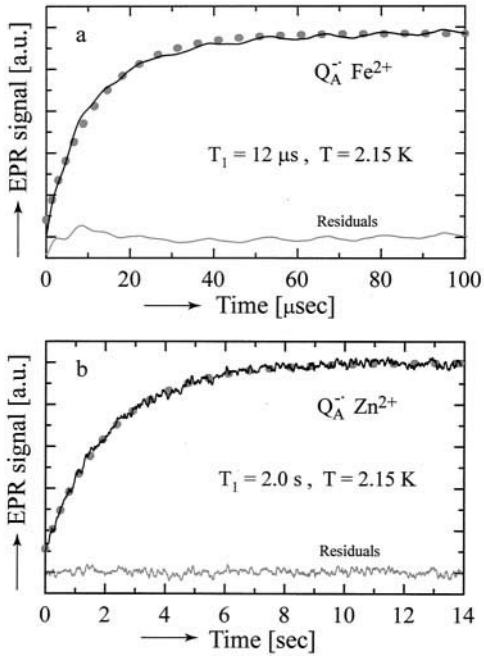

FIGURE 2 Recovery of the EPR signal (*solid lines*) after a saturating microwave pulse, observed at $\nu = 9$ GHz, and $T = 2.15$ K from (*a*) $Q_A^-Fe^{2+}$ and (*b*) $Q_A^-Zn^{2+}$. Data are fitted with a single exponential function (*gray dots*). The difference between the experimental curves and the fit (*i.e.*, residuals), are also shown. Note the difference in time scales of ~5 orders of magnitude between (*a*) and (*b*). The value of T_1 indicated in (*b*) is slightly shorter than the value extrapolated to zero power (see Fig. 4).

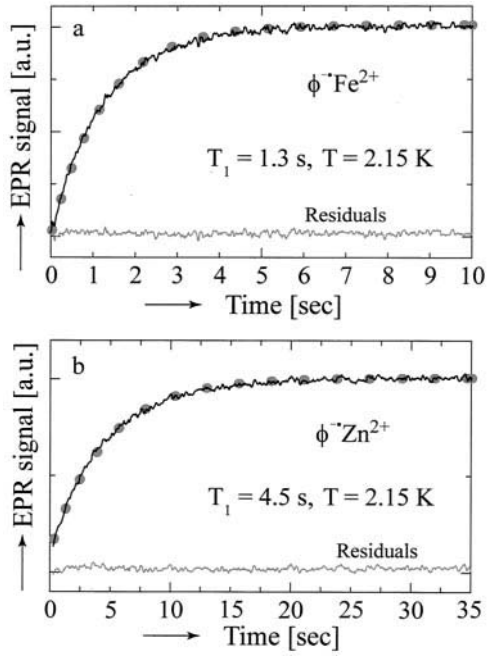

FIGURE 3 Recovery of the EPR signal (*solid lines*) after a saturating microwave pulse, observed at $\nu = 9$ GHz, and $T = 2.15$ K from (*a*) ϕ^-Fe^{2+}, (*b*) ϕ^-Zn^{2+}. Data are fitted with a single exponential function (*gray dots*). The difference between the experimental curves and the fit (*i.e.*, residuals) are also shown. The contribution of the Fe^{2+} ion to the relaxation of the ϕ^- spin is obtained by subtracting the rate determined in (*b*) from that in (*a*).

modulator. This scheme resulted in an improved reproducibility and baseline stability required for the signal averaging of the EPR recoveries. To minimize the 30 dB overload during the saturating microwave pulse a second HP 8735A pin diode modulator and by-pass arm in front of the 9 GHz preamp was used. The two modulators were adjusted to keep the overall gain of the system constant. The time response of the EPR signal was recorded with a LeCroy 9310M digital oscilloscope (LeCroy Corp, Chestnut Ridge, NY). The recovery signals were averaged on the oscilloscope and then transferred to a 450 MHz PC (Windows 2000) equipped with an AT-GPIB adapter card (National Instruments (NI), Austin, TX) running LabView 5.1 (NI). A Lab PC+ (NI) analog-to-digital acquisition card was used to control the magnetic field for EPR, and to supply various control signals. A solid metal TE_{102} cavity, constructed of high purity Al-Mg alloy (Al 95%-Mg 5%), which has a low paramagnetic background at liquid helium temperatures, was used. The electrical conductivity of this alloy does not increase on cooling to these temperatures, keeping a constant cavity Q of 4000 and allowing the use of field modulation up to 2 KHz.

Two ranges of values of T_1 were measured. For $Q_A^-Fe^{2+}$ and $Q_B^-Fe^{2+}$ T_1 was in the range of 1-20 μs. In this time domain, the recovery of the EPR signal was observed using field modulation with a boxcar integrator (Isaacson, 1968) connected to a lock-in amplifier (EG&G 7260 DSP, now Amertek, Inc., Oak Ridge, TN). In all other samples T_1 was longer than 100 ms and only the lock-in amplifier was used. In all cases many recoveries were averaged to improve the signal-to-noise (S/N) ratio. The relaxation time T_1 was defined as the 1/e time constant of the exponential recovery of the signal; it was calculated from the data using a commercial fitting program (Origin 6.1, OriginLab Corp., Northampton, MA). The possibility of multi-exponential recoveries was considered and is discussed later.

The sample of ϕ^-Fe^{2+} and all Zn^{2+}-containing samples have long relaxation times T_1 and are, therefore, easily saturated. The low microwave power required for no-saturation reduces the S/N ratio. To improve the S/N ratio we worked under slightly saturating conditions using higher microwave powers. To obtain T_1 under these conditions we used the relation (Slichter, 1990):

$$(1/T_1)_{\text{meas}} = 1/T_1 + \gamma W \qquad (1)$$

where W is the microwave power and γ is a constant that depends on experimental conditions. T_1 was obtained by measuring the EPR recovery, $(1/T_1)_{\text{meas}}$, as a function of W over a 9 dB range, and extrapolated to zero power at each temperature. This extrapolation is valid for single exponential decays, as was observed in all cases.

EXPERIMENTAL RESULTS

The temperature dependence of the relaxation time T_1 was measured at 9 GHz (X-band) between 1.4 and 4.2 K. For $Q_A^-Fe^{2+}$ and $Q_B^-Fe^{2+}$, the relaxation measurements were performed at a magnetic field **H** corresponding to the peak of the absorption χ'' signal ($g = 1.8$). In all other samples it was measured at the peaks of $d\chi''/dH$. The recovery of the signal following a saturating microwave pulse at 2.15 K is shown for $Q_A^-Fe^{2+}$ and $Q_A^-Zn^{2+}$ in Fig. 2, and for ϕ^-Fe^{2+} and ϕ^-Zn^{2+} in Fig. 3. The data are well fitted with a single exponential as seen from the small difference (residuals) between the observed and fitted curves. The results for $Q_B^-Fe^{2+}$ samples are similar to those for $Q_A^-Fe^{2+}$ (results not shown).

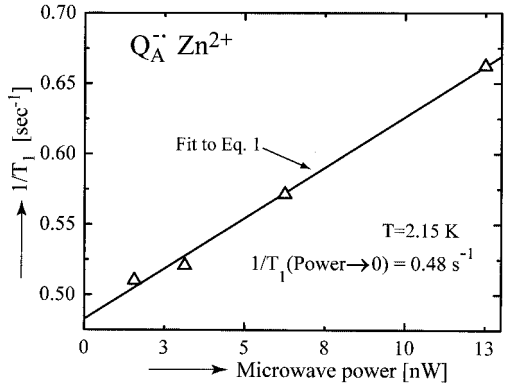

FIGURE 4 The observed relaxation rates $1/T_1$ for $Q_A^{\cdot-}Zn^{2+}$ at 2.15 K, at different microwave powers applied during the recovery phase. The solid line represents a fit to Eq. 1. Extrapolation to zero microwave power yields the inherent spin-lattice relaxation rate.

An example of the dependence of the measured recovery $(1/T_1)_{meas}$ on the microwave power W at 2.15 K is shown for $Q_A^{\cdot-}Zn^{2+}$ in Fig. 4. The value of $(1/T_1)$ is obtained by a linear extrapolation of the data to zero power (see Eq. 1).

The values of the relaxation rates $(1/T_1)$ as a function of temperature T measured between 1.4 and 4.2 K, for $Q_A^{\cdot-}Fe^{2+}$ and $Q_B^{\cdot-}Fe^{2+}$ are shown in Fig. 5 *a*, for $Q_A^{\cdot-}Zn^{2+}$ and for $Q_B^{\cdot-}Zn^{2+}$ in Fig. 5 *b*, and for $\phi^{\cdot-}Fe^{2+}$ and $\phi^{\cdot-}Zn^{2+}$ in Fig. 6. Each data point in Figs. 5 and 6 was obtained as described by Figs. 2–4.

The value of T_1 of $Q_A^{\cdot-}Fe^{2+}$ is ~5 orders of magnitude shorter than that observed in $Q_A^{\cdot-}Zn^{2+}$ (Fig. 5, *a* and *b*).

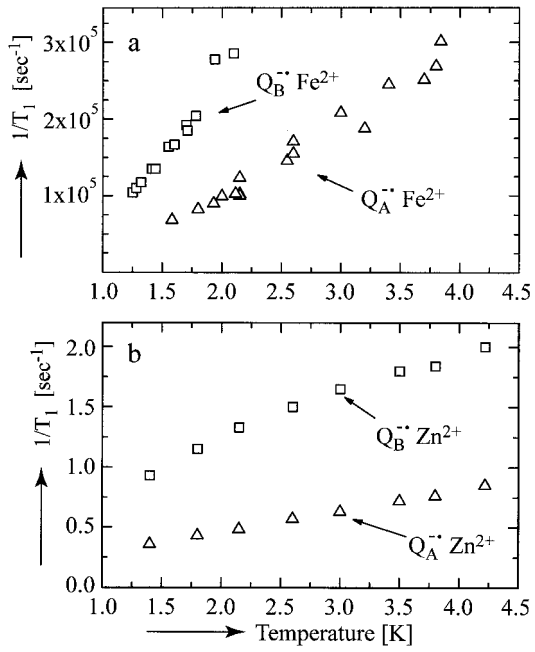

FIGURE 5 Temperature dependence of the observed relaxation rate $1/T_1$ at $\nu = 9$ GHz for (*a*) $Q_A^{\cdot-}Fe^{2+}$ and $Q_B^{\cdot-}Fe^{2+}$, (*b*) $Q_A^{\cdot-}Zn^{2+}$ and $Q_B^{\cdot-}Zn^{2+}$.

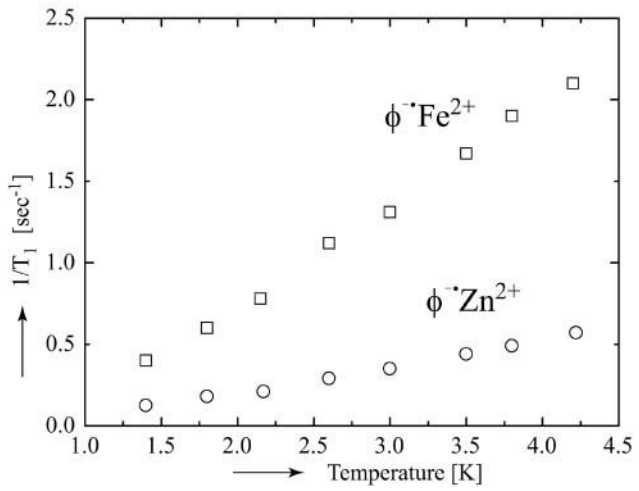

FIGURE 6 Temperature dependence of the observed relaxation rate $1/T_1$ at $\nu = 9$ GHz for $\phi^{\cdot-}Fe^{2+}$ and $\phi^{\cdot-}Zn^{2+}$.

Similar results were obtained for $Q_B^{\cdot-}Fe^{2+}$. The value of T_1 of $\phi^{\cdot-}Fe^{2+}$ is shorter than that observed in $\phi^{\cdot-}Zn^{2+}$ (Fig. 6), but the difference is much smaller than for the quinones. These results confirm the role of the Fe^{2+} ion in the relaxation of the cofactors. The effect of the Fe^{2+} is much more pronounced for the quinone acceptors $Q_A^{\cdot-}$ and $Q_B^{\cdot-}$, which are closer to the Fe^{2+} ion than $\phi^{\cdot-}$ (see Fig. 1).

THEORY

Spin-Hamiltonian description of the spin-dimer

The spins of each oxidized or reduced cofactor **s** (s = 1/2) that participate in the electron transfer chain of the photosynthetic reaction center and the Fe^{2+} spin **S** (S = 2) give rise to a coupled spin-dimer. The spin-spin interaction between **s** and **S** is described by the Hamiltonian:

$$H_{sS} = -\mathbf{s} \cdot \mathbf{J} \cdot \mathbf{S} \qquad (2)$$

where **J** is the interaction tensor. In simple cases **J** is isotropic, and Eq. 2 gives the Heisenberg exchange ($-J_o\mathbf{s} \cdot \mathbf{S}$) described by a single, scalar, quantity J_o. Anisotropic contributions to **J** in Eq. 2 can arise from dipolar interactions or from higher order exchange terms (Bencini and Gatteschi, 1990). Antisymmetric exchange can arise from higher order contributions of the spin-orbit interaction (Moriya, 1960). Both of these exchange contributions are usually smaller than the isotropic value J_o. Furthermore, we will show that only one term in Eq. 2 contributes to the relaxation of the cofactors in the RC, and thus anisotropies are not relevant for this work.

The spin-Hamiltonian H_s describing the properties of the Fe^{2+}-Cof spin-dimer (Cof stands for the cofactors $Q_A^{\cdot-}$, $Q_B^{\cdot-}$, and $\phi^{\cdot-}$ of the photosynthetic RC) in an external mag-

netic field **H**, can be written as (Abragam and Bleaney, 1970; Butler et al., 1980, 1984):

$$H_s = D[S_z^2 - S(S+1)/3] + E(S_x^2 - S_y^2) + \mu_B \mathbf{H}\cdot\mathbf{g}_{Fe}\cdot\mathbf{S} + \mu_B g_{Cof}\mathbf{H}\cdot\mathbf{s} + H_{sS} \quad (3)$$

where D and E are zero field splitting parameters of the Fe^{2+}; $\mathbf{g}_{Fe}$ is the g-tensor of the Fe^{2+} spin, g_{Cof} is the g-factor of **s**. These g-values are close to being isotropic, which justifies taking their average values, $g_{Cof} \approx 2.0046$ for Q_A^- and Q_B^- (Isaacson et al., 1995), and $g_{Cof} \approx 2.0036$ for ϕ^- (Okamura et al., 1979b). μ_B is the Bohr magneton, and H_{sS} is given by Eq. 2. Equation 3 is written in the coordinate axes in which the zero field splitting is diagonal, and characterized by D and E. When the Fe^{2+} is replaced by diamagnetic Zn^{2+}, the terms of Eq. 3 involving **S** are zero. The best characterized RC spin-dimer is $Q_A^-Fe^{2+}$ in *Rb. sphaeroides* (Butler et al., 1980, 1984), for which the values of the parameters are:

$$D/k_B = 7.6\ \text{K}, \quad E/k_B = 1.9\ \text{K},$$
$$g_{Fe,x} = 2.16, \quad g_{Fe,y} = 2.27, \quad \text{and} \quad g_{Fe,z} = 2.04,$$
$$J_x/k_B = -0.13\ \text{K}, \quad J_y/k_B = -0.58\ \text{K},$$
$$\text{and} \quad J_z/k_B = -0.58\ \text{K} \quad (4)$$

where it was assumed that the principal axes of the exchange interaction and the zero field splitting tensor are the same. It is expected that the values of D, E, and the components of the **g**-tensor of Fe^{2+} do not change for $Q_B^-Fe^{2+}$ and ϕ^-Fe^{2+}. However, the values of **J** will be different for the different cofactors.

The levels scheme predicted by Eq. 3 with the parameters for the dimer $Q_A^-Fe^{2+}$ given in Eq. 4 is shown in Fig. 7 *a* (Butler et al., 1984). The fivefold $(2S + 1)$ degeneracy of the energy levels of the $S = 2$ spin of the Fe^{2+} ion is split by the terms D and E in Eq. 3. The first and second excited levels are 3.2 K and 15 K above the ground state. Each of the five levels has a twofold degeneracy due to the spin of the cofactor radical. This degeneracy is split by the external field **H**, as shown in Fig. 7 *a* for a magnetic field applied along the *y*-direction, which is defined by the zero field splitting terms of the spin Hamiltonian in Eq. 3. The EPR signal centered at $g \approx 1.8$ observed at helium temperatures in randomly oriented frozen $Q_A^-Fe^{2+}$ dimers is a superposition of the EPR signals arising from the ground state doublet (the high field side), and from the excited state doublet (the low field side), as shown in Fig. 7 *b* (Butler et al., 1984). The main feature of both contributions to the spectrum of $Q_A^-Fe^{2+}$ is a strong anisotropy of the g-tensor, with the principal g-value along the y-direction (g_y) considerably displaced from g_x and g_z (g_x and g_z are close to the center of the line at $g \sim 1.8$). This is a consequence of the large magnetic moment induced in the two lowest states of the Fe^{2+} ion when the external magnetic field is applied along the y-direction (Butler et al., 1984). The other three doublets are not populated in the temperature range at which the EPR spectra were observed, and therefore do not contribute. The spectrum in Fig. 7 *b* corresponds to $Q_A^-Fe^{2+}$; similar results were obtained for $Q_B^-Fe^{2+}$. For the ϕ^-Fe^{2+} dimer, the spin-spin interaction is much smaller, and the effect of the zero field splitting is buried in the width of the ϕ^- signal, which is mainly due to hyperfine interactions with the proton nuclei.

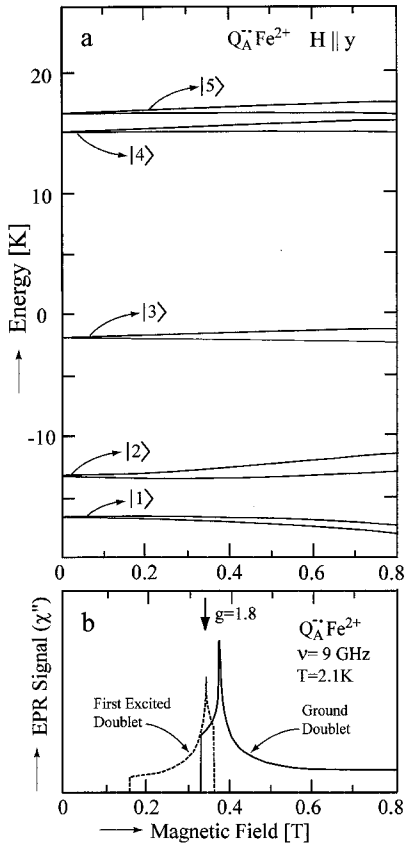

FIGURE 7 (*a*) Energy levels of the spin-dimer $Q_A^-Fe^{2+}$, obtained from Eq. 3 with the magnetic field H applied along the *y*-axis of the crystal field. The spin $S = 2$ of the iron ion gives rise to five energy levels, each being twofold degenerate due to the interaction with the spin $s = ½$ of the cofactor. (*b*) Contributions of the two lowest doublets to the EPR spectrum observed at $\nu = 9$ GHz and 2.1 K. Modified from Butler et al. (1984).

Spin-lattice relaxation of a coupled dimer

We present now a model that explains our spin-lattice relaxation data. Details of the calculations are given in Appendix A.

The spin-lattice interaction

To calculate the spin-lattice relaxation of the coupled dimer we add to Eq. 3 the spin-lattice interactions $H_{sl}(\mathbf{s})$, acting on

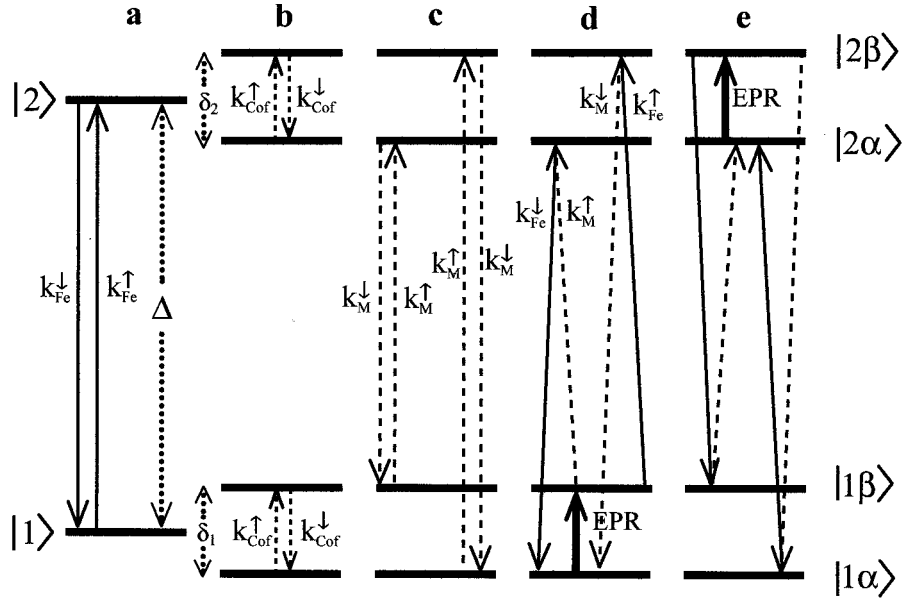

FIGURE 8 The two lowest doublet states of the $Q^{-}Fe^{2+}$ spin-dimer and the transitions between them. (*a*) The Fe^{2+} levels with a splitting Δ (*dotted double arrow*) at zero magnetic field. The spin-lattice transitions proceed with rates $k_{Fe}^{\uparrow}$ and $k_{Fe}^{\downarrow}$ (*solid arrows*). (*b*) Application of a magnetic field splits the Fe^{2+} levels due to the spin of Q^{-} by an amount δ (*dotted double arrow*). The direct relaxation of Q^{-} proceeds with rates $k_{Cof}^{\uparrow}$ and $k_{Cof}^{\downarrow}$. (*c*) Spin-lattice transitions $k_{M}^{\uparrow}$ and $k_{M}^{\downarrow}$ (*dashed arrows*) that change the states of both spins (**s** and **S**). (*d*) Two-phonon transitions with rates k_M and k_{Fe}, respectively, produce a net relaxation of the spins in the lowest doublet. (*e*) Same as (*d*) for the higher doublet. The EPR transitions are indicated by heavy arrows.

the spin of the cofactor, and $H_{Sl}(\mathbf{S})$, acting on the Fe^{2+} spin. They couple **s** and **S**, respectively, to the electric field produced by the local distortions associated with the thermal vibrations (see Appendix A). Adding to Eq. 3 the interaction of the spin-dimer with the thermal vibrations we obtain:

$$H = H_s + H_{sl}(\mathbf{s}) + H_{Sl}(\mathbf{S}) \tag{5}$$

$H_{Sl}(\mathbf{S})$ induces transitions between the five levels of **S**, with the absorption and emission of phonons. Since Fe^{2+} is a non-Kramers' ion (even number of electrons), its energy levels are split by the crystalline *electric* field. $H_{Sl}(\mathbf{S})$, therefore, couples directly to the lattice vibrations, making Fe^{2+} a *fast relaxer* (Shiren, 1962, 1963; Watkins and Feher, 1962). The cofactors, however, having a spin of ½, are purely *magnetic* entities (Kramers' doublet) and relax only in the presence of **H** through admixtures of higher levels through spin-orbit interactions (Van Vleck, 1940; Abragam and Bleaney, 1970; Orbach and Stapleton, 1972). Consequently, $H_{sl}(\mathbf{s})$ produces a weak interaction making the cofactors *slow relaxers*.

Interlevel Transition Rates

Fig. 8, *a–e* focuses on the two lower doublet states displayed in Fig. 7 *a*. Only these two levels are populated below 4.2 K and are, therefore, responsible for the low temperature EPR spectrum and relaxation processes of $Q_A^{-}Fe^{2+}$ (Fig. 7 *b*). Fig. 8 *a* shows the two lowest energy levels of an isolated Fe^{2+} ion that are separated by the zero field splitting Δ (*dotted line*). The solid arrows indicate transitions between the energy states $|1\rangle$ and $|2\rangle$ produced by $H_{Sl}(\mathbf{S})$ with rates $k_{Fe}^{\uparrow}$ and $k_{Fe}^{\downarrow}$, with the absorption and emission of phonons, respectively. No EPR transition between these two levels are induced at the employed microwave frequencies and magnetic fields and, therefore, the Fe^{2+} ion is EPR silent in unreduced RCs. Fig. 8 *b* includes the splittings δ_1 and δ_2 of the Fe^{2+} levels produced by its coupling with the s = 1/2 spin of the cofactor. For simplicity, we assume that $\delta_1 \approx \delta_2 = \delta$. Dashed arrows labeled with rates $k_{Cof}^{\uparrow}$ and $k_{Cof}^{\downarrow}$ indicate spin-lattice transitions produced by $H_{sl}(\mathbf{s})$. These transitions change the spin state of **s** (from $|\alpha\rangle$ to $|\beta\rangle$ or vice-versa), with the absorption or emission of phonons, without changing the spin state of **S** ($|1\rangle$ and $|2\rangle$). Fig. 8 *c* considers transitions labeled $k_{M}^{\uparrow}$ and $k_{M}^{\downarrow}$ that change the spin states of both **s** and **S**. A quantum mechanical calculation of k_M, produced by $H_{Sl}(\mathbf{S})$ in the presence of H_{sS}, is given in Appendix A. The thick solid arrows in Fig. 8, *d* and *e* indicate the transitions induced by the microwave field, which give rise to the observed EPR signal (Fig. 7 *b*). Fig. 8, *d* and *e* also show the pairs of transitions contributing to the two phonon relaxation processes for each of the two doublets with solid and dashed arrows. Each doublet relaxes via two phonons characterized by rates $k_{M}^{\uparrow}$ and $k_{Fe}^{\downarrow}$, or $k_{M}^{\downarrow}$ and $k_{Fe}^{\uparrow}$ (Fig. 8, *d* and *e*). These processes are much more effective than those produced by k_{Cof} (Fig. 8 *b*).

The values of the transition rates are (Abragam and Bleaney, 1970) (see Appendix A):

$$k_{Cof}^{\uparrow} = A_{Cof} n_{\delta}, \quad k_{Cof}^{\downarrow} = A_{Cof}(n_{\delta} + 1) \tag{6a}$$

$$k_{Fe}^{\uparrow} = A_{Fe} n_{\Delta}, \quad k_{Fe}^{\downarrow} = A_{Fe}(n_{\Delta} + 1) \tag{6b}$$

$$k_{M}^{\uparrow} = A_{M} n_{\Delta\pm\delta}, \quad k_{M}^{\downarrow} = A_{M}(n_{\Delta\pm\delta} + 1) \tag{6c}$$

where n_{δ}, n_{Δ}, and $n_{\Delta\pm\delta}$ are the equilibrium populations of the phonons with energies $x = \delta$, Δ and $\Delta \pm \delta$, respectively.

They are given at temperature T by the phonon occupancy numbers (Bose factors), $n_x = (\exp(x/k_BT) - 1)^{-1}$. A_{Cof}, A_{Fe}, and A_M represent the strength of the interactions giving rise to each of the processes displayed in Fig. 8, *a* and *c*. The magnitudes of A_{Fe} and A_{Cof} involve elastic constants (or sound velocities), phonon densities appropriate to the protein at the site of the spin-dimer, and matrix elements of $H_{Sl}(\mathbf{S})$ and $H_{sl}(\mathbf{s})$ (see Appendix A), respectively (Van Vleck, 1940; Orbach, 1961; Abragam and Bleaney, 1970). We show in Appendix A that A_M is proportional to A_{Fe}, the proportionality constant involving components of **J** (Eq. 2) and the crystal field splitting parameters of the Fe^{2+} ion (Eqs. 3 and 4).

Relaxation rate $(1/\tau)_{Fe}$ of the Fe^{2+} ion

Let N_1 and N_2 be the populations of levels $|1\rangle$ and $|2\rangle$ in Fig. 8 *a*. The rate equations for N_1 and N_2 arising from $k_{Fe}^{\uparrow}$ and $k_{Fe}^{\downarrow}$ are:

$$dN_1/dt = -dN_2/dt = -k_{Fe}^{\uparrow}N_1 + k_{Fe}^{\downarrow}N_2 \qquad (7)$$

Using Eqs. 6b and 7 and the condition $(N_1)_{eq}\, k_{Fe}^{\uparrow} = (N_2)_{eq}\, k_{Fe}^{\downarrow}$ for the equilibrium populations $(N_1)_{eq}$ and $(N_2)_{eq}$, we obtain (Abragam and Bleaney, 1970):

$$d(N_1 - N_2)/dt = -(1/\tau)_{Fe}[(N_1 - N_2) - (N_1 - N_2)_{eq}] \qquad (8)$$

for the relaxation of the two lowest levels of the Fe^{2+} ion. Equation 8 shows that as $t \rightarrow \infty$, $(N_1 - N_2)$ approaches exponentially its thermal equilibrium value $(N_1 - N_2)_{eq} = (N_1 + N_2)\tanh(\Delta/2k_BT)$ with a characteristic time τ_{Fe} defined by:

$$(1/\tau_{Fe}) = k_{Fe}^{\uparrow} + k_{Fe}^{\downarrow} = A_{Fe}(2n_\Delta + 1) \qquad (9)$$

The temperature dependence of τ_{Fe} enters into Eq. 9 through the phonon occupancy factor n_Δ. This equation is valid at low temperatures where only phonon transitions involving the two lowest levels of the Fe^{2+} ion contribute to the relaxation (Van Vleck, 1940; Abragam and Bleaney, 1970). At higher temperatures, when other excited levels of the Fe^{2+} ion are populated, Eq. 8 needs to be replaced by a set of coupled differential equations that give rise to $(m - 1)$ relaxation times, where m is the number of populated Fe^{2+} levels (see Appendix B).

Relaxation rate of the cofactors in the presence of spin-spin coupling

Let $N_{1\alpha}$, $N_{1\beta}$, $N_{2\alpha}$, and $N_{2\beta}$ be the populations of the states $|1\alpha\rangle$, $|1\beta\rangle$, $|2\alpha\rangle$ and $|2\beta\rangle$ shown in Fig. 8. At low temperatures, when only these levels are populated, the total number N of dimers is,

$$N = N_{1\alpha} + N_{1\beta} + N_{2\alpha} + N_{2\beta} \qquad (10)$$

From Fig. 8 and Eqs. 6, the rate equation for $N_{1\alpha}$ is:

$$\begin{aligned} dN_{1\alpha}/dt = &- A_{Cof}n_\delta N_{1\alpha} + A_{Cof}(n_\delta + 1)N_{1\beta} \\ &- A_M n_{\Delta+\delta} N_{1\alpha} + A_M(n_{\Delta+\delta} + 1)N_{2\beta} \\ &- A_{Fe}n_\Delta N_{1\alpha} + A_{Fe}(n_\Delta + 1)N_{2\alpha} \end{aligned}$$

Similar rate equations may be written for $N_{1\beta}$, $N_{2\alpha}$, and $N_{2\beta}$. The differences in populations of the spin up states $|\alpha\rangle$ and spin down states $|\beta\rangle$ that give rise to the EPR transitions (Fig. 8 *b*) are:

$$\begin{aligned} &d(N_{1\alpha} - N_{1\beta})/dt \\ &= - 2A_{Cof}n_\delta(N_{1\alpha} - N_{1\beta}) + 2A_{Cof}N_{1\beta} \\ &\quad - A_M n_{\Delta+\delta}(N_{1\alpha} - N_{2\beta}) \\ &\quad - A_M n_{\Delta-\delta}(N_{2\alpha} - N_{1\beta}) \\ &\quad - A_M(N_{2\alpha} - N_{2\beta}) - A_{Fe}n_\Delta(N_{1\alpha} - N_{1\beta}) \\ &\quad + A_{Fe}(n_\Delta + 1)(N_{2\alpha} - N_{2\beta}) \end{aligned} \qquad (11)$$

and,

$$\begin{aligned} d(N_{2\alpha} - N_{2\beta})/dt = &- 2A_{Cof}n_\delta(N_{2\alpha} - N_{2\beta}) + 2A_{Cof}N_{2\beta} \\ &- A_M n_{\Delta-\delta}(N_{2\alpha} - N_{1\beta}) \\ &- A_M n_{\Delta+\delta}(N_{1\alpha} - N_{2\beta}) \\ &- A_M(N_{2\alpha} - N_{2\beta}) \\ &- A_{Fe}(n_\Delta + 1)(N_{2\alpha} - N_{2\beta}) \\ &+ A_{Fe}n_\Delta(N_{1\alpha} - N_{1\beta}) \end{aligned} \qquad (12)$$

The recovery of the EPR signal was measured at the peak of the absorption, where transitions from both doublets contribute. The relevant rate equation is therefore given by the sum of Eqs. 11 and 12.

$$\begin{aligned} dn/dt = &- 2A_{Cof}n_\delta n - 2A_{Cof}(N_{1\beta} + N_{2\beta}) \\ &- 2A_M n_{\Delta+\delta}(N_{1\alpha} - N_{2\beta}) \\ &- 2A_M n_{\Delta-\delta}(N_{2\alpha} - N_{1\beta}) \\ &- 2A_M(N_{2\alpha} - N_{2\beta}) \end{aligned} \qquad (13)$$

where α and β refer to the spin states of the cofactor and $n = N_\alpha - N_\beta$, with $N_\alpha = N_{1\alpha} + N_{2\alpha}$ and $N_\beta = N_{1\beta} + N_{2\beta}$.

For $A_{Fe}n_\Delta \gg A_{Cof}n_\delta$, and $A_{Fe}n_\Delta \gg A_M n_{\Delta\pm\delta}$, a fast thermal equilibrium is reached between the populations $N_{1\alpha}$ and $N_{2\alpha}$ and between $N_{1\beta}$ and $N_{2\beta}$. Thus, at times much shorter than the relaxation time of the cofactors, the following Boltzmann equilibrium conditions hold:

$$N_{2\alpha}/N_{1\alpha} = N_{2\beta}/N_{1\beta} = \exp(-\Delta/k_BT) \qquad (14)$$

From Eqs. 13 and 14 and the condition that N remains constant at low T (Eq. 10), there is only one independent

rate equation for the four levels system of Fig. 8. For $\Delta \gg \delta$, i.e., $\Delta \pm \delta \approx \Delta$:

$$\frac{dn}{dt} = \left[-A_{Cof}(2n_\delta + 1) - 2A_M n_\Delta - \frac{2A_M}{\exp(\Delta/k_BT) + 1} \right] \times (n - n_0) = (1/T_1)_{obs}(n - n_0) \quad (15)$$

where n_0 is the equilibrium value of n at long times, when $dn/dt = 0$. In the experiments reported here, a high-power microwave pulse saturates the populations (i.e., produces $N_\alpha = N_\beta$). $(1/T_1)_{obs}$ is the observed relaxation rate of the cofactor. For $\delta \ll k_BT$, $n_\delta \approx k_BT/\delta$. From Eq. 15:

$$(1/T_1)_{obs} = 2A_{Cof}k_BT/\delta + \frac{4A_M\exp(\Delta/k_BT)}{\exp(2\Delta/k_BT) - 1} = (1/T_1)_{int} + (1/T_1)_M \quad (16)$$

Equation 16 shows two contributions to $(1/T_1)_{obs}$. The intrinsic contribution $(1/T_1)_{int}$ is produced by the spin-lattice interaction $H_{sl}(\mathbf{s})$ between the radical spins and the local vibrations of the protein by a direct process. Its magnitude is proportional to A_{Cof}. The magnetic contribution, $(1/T_1)_M$, proceeds through the spin-spin interaction between the metal ion and the cofactor, and its magnitude is proportional to A_M. The approximations in Eq. 10 (only the two lowest doublets are populated) and Eq. 14 (the relaxation of Fe^{2+} is much faster than that of the cofactors) lead to a single exponential recovery, given by Eq. 16. Without these approximations multiple-exponential recoveries would be observed (see Appendix B).

The value of A_{Cof} in Eq. 16 involves matrix elements within Kramers' doublets and density of phonons with energy δ. A_M involves matrix elements within the orbital degenerate levels of the iron and the density of phonons with energy $\sim\Delta$. When $A_M n_\Delta \gg A_{Cof} n_\delta$, and as $A_M \ll A_{Fe}$, we can neglect the term containing A_{Cof} in Eq. 16 and obtain:

$$\mathbf{(1/T_1)_{obs}} \approx (1/T_1)_M = \frac{4A_M\exp(\Delta/k_BT)}{\exp(2\Delta/k_BT)} = \frac{\mathbf{2A_M}}{\mathbf{\sinh(\Delta/k_BT)}} \quad (17)$$

However, when the intrinsic and magnetic contributions to the relaxation rate of Eq. 16 have similar magnitudes (e.g., in the case of the ϕ-Fe^{2+} dimers), $(1/T_1)_M$ is obtained from the experimental values $(1/T_1)_{obs}$ by subtracting the intrinsic contribution $(1/T_1)_{int}$ measured in the ϕ-Zn^{2+} sample (Eq. 16).

The relaxation mechanism leading to $(1/T_1)_M$ in Eq. 17 involves two phonons (see Fig. 8, *d* and *e*). One is absorbed and the other is emitted. In one step (labeled k_M), a phonon produces a change of the quantum numbers of both **S** and **s**. In the step labeled k_{Fe} only **S** changes. The net result is a change of the quantum number of **s**, i.e., a flip of the cofactor spin $|\alpha\rangle \leftrightarrow |\beta\rangle$. The transition probability of simultaneously flipping two spins (*S* and *s*) is smaller than flipping only the spin S, i.e., $A_M \ll A_{Fe}$ (see Appendix A). Consequently, the relaxation rate $(T_1)_M$ is essentially determined by A_M. This relaxation process for the cofactors is similar to that proposed by Orbach (1961) for rare earth ions having low excited energy states.

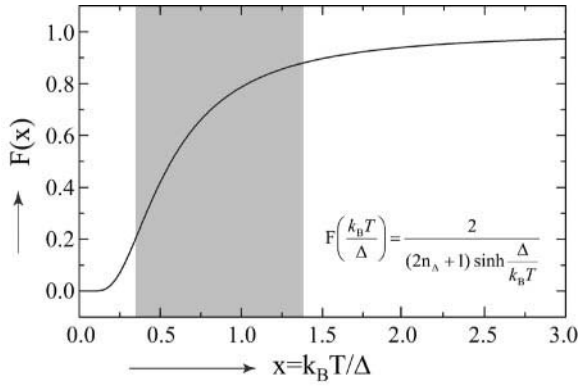

FIGURE 9 The function $F(x)$ defined by Eq. 19 plotted versus $x = k_BT/\Delta$. The range of x covered in our experiments is indicated by the gray area.

The two-phonon transitions that effectively flip the spin of the cofactor occur between the Fe^{2+} levels split by the crystal field. The energies of these transitions are much larger than those between the magnetic levels of the cofactors. Because the phonon density is proportional to the square of the energy (Kittel, 1996) and the matrix element of $H_{SI}(\mathbf{S})$ is larger than that of $H_{sl}(\mathbf{s})$, the two-phonon mechanism is more efficient in relaxing the cofactor spin than the direct relaxation of **s**.

Ratio between the spin-lattice relaxation rates of the iron and the cofactors

The ratio between the relaxation time for the Fe^{2+} ion $(\tau)_{Fe}$ (Eq. 9) and the relaxation time $(T_1)_M$, predicted by the two-phonon model (Eq. 17) is:

$$R = \frac{\tau_{Fe}}{(T_1)_M} = \frac{2A_M}{\sinh(\Delta/k_BT)} \frac{1}{A_{Fe}(2n_\Delta + 1)} = \frac{A_M}{A_{Fe}} F(k_BT/\Delta) \quad (18)$$

The function:

$$F(k_BT/\Delta) = \frac{2}{\sinh(\Delta/k_BT)(2n_\Delta + 1)} \quad (19)$$

is plotted versus k_BT/Δ in Fig. 9. For $k_BT \ll \Delta$, $F(k_BT/\Delta) \approx 0$ and $R \approx 0$ (*e.g.*, $(T_1)_M \rightarrow \infty$), showing that at very low temperatures the two-phonon relaxation mechanism leading to Eq. 17 is not effective. This is because when $k_BT \ll \Delta$ there are few phonons with energy Δ to be absorbed. However, the relaxation of the iron giving rise to $(1/\tau)_{Fe}$ is still

effective because it utilizes the emission of phonons. For $k_BT/\Delta \geq 2$, $F(k_BT/\Delta) \approx 1$, *i.e.*, $R = A_M/A_{Fe}$, independent of T, and the two phonon mechanism leading to Eq. 17 is most effective. At the highest temperature used in our experiments (4.2 K), $k_BT/\Delta = 0.27$ for the second excited state ($|3\rangle$ in Fig. 7 *a*), resulting in $F(k_BT/\Delta) \approx 0.1$, which justifies our neglect of higher excited states in our analysis.

The ratio A_M/A_{Fe} in terms of measured quantities is given by Eq. A6,

$$\frac{A_M}{A_{Fe}} = \frac{J_y^2 P^2}{2\Delta^2} \tag{20}$$

where J_y is the magnitude of the *y*-component of **J**, which includes exchange and dipolar contributions, and P depends on the rhombicity E/D of the Fe^{2+} ion (Butler et al., 1984) (defined in Eq. A4). Separate values of A_{Fe} and A_M are difficult to calculate; they involve elastic properties (sound velocities), local density, and density of phonons of the protein (see Eq. A2). In view of the difficulties in estimating these values, we consider only the change of the magnetic interaction between the Fe^{2+} and the different cofactors. We make the reasonable assumption that all the other parameters are the same for Q_A^-, Q_B^-, and ϕ^-. From Eqs. 18 and 20 we obtain:

$$1/(T_1)_M = \frac{J_y^2 P^2}{2\Delta^2} F(k_BT/\Delta)(1/\tau_{Fe}) \tag{21}$$

Using the values $P = 1.9$ (obtained for $E/D = 0.25$), $\Delta/k_B = 3.2$ K, and $J_y/k_B = -0.58$K, appropriate for $Q_A^-Fe^{2+}$ (Butler et al., 1984), we obtain from Eq. 21:

$$1/(T_1)_M \cong \frac{1}{17} F(k_BT/\Delta)(1/\tau_{Fe}) \tag{22}$$

Thus, according to our model, the relaxation time T_1 observed for $Q_A^-Fe^{2+}$ at $T \approx 4$ K is 17 times longer than that of Fe^{2+} (Eq. 22). In this case it is clearly valid to neglect A_{Cof} in Eq. 16 to obtain Eq. 17. For ϕ^-, whose distance to the Fe^{2+} ion is larger and thus $|J_y|$ is smaller, the contribution $1/(T_1)_M$ to the observed relaxation rate is of the same order as the intrinsic relaxation rate, and has to be evaluated from data obtained from both ϕ^-Fe^{2+} and ϕ^-Zn^{2+}.

Equation 21 shows that only the *y*-component of the spin-spin interaction **J** contributes to the relaxation rate. This result is a consequence of the rhombicity (E/D = 0.25) of the crystal field-splitting of the Fe^{2+} spin and has been previously discussed by Butler et al. (1984). A magnetic field along *y* induces a large magnetic moment in each of the two lowest Fe^{2+} energy levels, and consequently gives rise to a large magnetic field at the spin of the cofactors. This magnetic field is time dependent due to the relaxation of the Fe^{2+} spin, and is responsible for the relaxation of the cofactors spins. Fields along *x* and *z* produce much smaller magnetic moments, and consequently J_x and J_z are less effective in relaxing the cofactor spins.

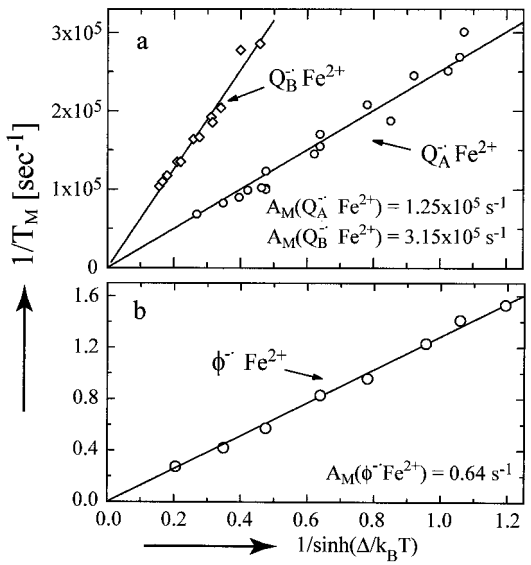

FIGURE 10 The magnetic contribution ($1/T_M$) to the relaxation rates for (*a*) $Q_A^-Fe^{2+}$ and $Q_B^-Fe^{2+}$; (*b*) ϕ^-Fe^{2+}. The circles are experimental points obtained from the data in Figs. 5 and 6 using Eq. 23. Solid lines are fits of the data with Eq. 17, using $\Delta/k_B = 3.2$ K (Butler et al., 1984).

ANALYSIS OF THE DATA AND DISCUSSION

Analysis of the relaxation data in terms of the spin-dimer model

We start by determining the contribution of the Fe^{2+}, $(1/T_1)_M$, to the relaxation of the cofactors Q_A^-, Q_B^-, and ϕ^-. This is achieved by subtracting from the relaxation rate $(1/T_1)_{obs}$ observed in Fe^{2+} containing RCs, the intrinsic relaxation rate $(1/T_1)_{int}$ obtained in Zn^{2+} containing RCs, *i.e.*:

$$(1/T_1)_M = (1/T_1)_{obs} - (1/T_1)_{int} \tag{23}$$

For $Q_A^-Fe^{2+}$ and $Q_B^-Fe^{2+}$, $(1/T_1)_{obs} \gg (1/T_1)_{int}$ and $(1/T_1)_{obs} = (1/T_1)_M$. For ϕ^-Fe^{2+}, $(1/T_1)_{obs}$ and $(1/T_1)_{int}$ are of the same order of magnitude and Eq. 23 has to be used.

To compare the experimentally determined relaxation rate $(1/T_1)_M$ with the spin dimer model, we plot $(1/T_1)_M$ as a function of $1/\sinh(\Delta/k_BT)$ using a value of $\Delta/k_B = 3.2$ K (Butler et al., 1984). Equation 17 predicts a linear relation. This is observed for all three cofactors, Q_A^- and Q_B^-, and for ϕ^- (see Fig. 10, *a* and *b*), which provides strong evidence for the validity of the model. From the slope of the lines, a value of A_M for each cofactor was evaluated (see Table 1). We also performed the fit leaving both A_M and Δ as independent parameters. The values of Δ obtained in this way differed in all cases by <20% from the previously determined value, adding additional evidence to the validity of the model. However, the strong correlation between the parameters Δ and A_M in Eq. 17 introduces inaccuracies that exceed the error of the previously determined Δ (Butler et

TABLE 1 Spin-spin interactions between the Fe^{2+} ion and the cofactors, and between cofactors in reaction centers from photosynthetic bacteria

Spin-Dimer	A_M [s^{-1}]	$\|J_o\|/k_B$ [K]	Distance [Å]	Reference
Metal-cofactor spin dimers				
$Q_A^-Fe^{2+}$ (*Rb. sphaeroides*)	$(1.25 \pm 0.03) \times 10^5$	0.58	8.8	Butler et al. (1984)
$Q_B^-Fe^{2+}$ (*Rb. sphaeroides*)	$(3.15 \pm 0.05) \times 10^5$	0.92	8.7	This work
ϕ^-Fe^{2+} (*Rb. sphaeroides*)	(0.64 ± 0.01)	1.3×10^{-3}	18.3	This work
ϕ^-Fe^{2+} (*Rb. viridis*)	—	9×10^{-4}	18.1	Van den Brink et al. (1996)*
Cofactor-cofactor spin-dimers				
$\phi^-Q_A^-$ (*Rb. sphaeroides*)		8×10^{-3}	13.9	Okamura et al. (1979b)†
$\phi^-Q_A^-$ (*Rb. viridis*)		2×10^{-2}	13.2	Van den Brink et al. (1996)*
$D^+Q_A^-$ (*Rb. sphaeroides*)		$<1 \times 10^{-4}$	28.8	Zech et al. (1996)
$Q_A^-Q_B^-$ (*Rb. sphaeroides*)		3.9×10^{-3}	17.3	Calvo et al. (2001)
$D^+\phi^-$ (*Rb. sphaeroides*)		$1.3 \times 10^{-3.5\pm0.5}$	19.3	Moehl et al. (1985), Ogrodnik et al. (1987)

Distances between the interacting spins were obtained for *Rb. sphaeroides* from the structure by Stowell et al. (1997) and for *R. viridis* by Deisenhofer et al. (1995). Distances were taken at the centers of the ring of Q_A^-, Q_B^-, and ϕ^- radicals and for D^+ at the point bisecting the line connecting the two Mg^{2+} atoms of the bacteriochlorophyll dimer.

*The definition of J_o in their work differed from ours by a factor of 2. We adjusted their value to correspond to our definition.

†In this case Q_A^- was a menaquinone that replaced the native ubiquinone-10.

al., 1984). We, therefore, used $\Delta/k_B = 3.2$ K as a fixed, known, parameter.

Comparison of the proposed spin-dimer model with previous models

The basic ideas of relaxing a slow (nuclear) spin through a fast-relaxing (electronic) spin were introduced by Bloembergen et al. (1948, 1949, 1961) and extended by Abragam (1955, 1961). In their model, the slow spin "sees" a time dependent magnetic field having a Lorentzian frequency spectrum with a width determined by the relaxation time of the fast spin. The Fourier component of the spectrum of the fast spin at the Larmor frequency of the slow spin induces transitions that shorten the relaxation time of the slow spin. The theory predicts a relaxation rate of the slow spin proportional to the square of the spin-spin interaction between the two spins.

The above model was extended by Kulikov and Likhtenstein (1977) and Hyde et al. (1979) to the relaxation of a slow electronic spin (e.g., free radical) magnetically interacting with a fast electronic spin (e.g., transition metal ion). It was applied by several authors to investigate the relaxation rate of cofactor radicals in bacterial photosynthetic RCs (Bowman et al., 1979; Norris et al., 1980; Hirsh and Brudvig, 1993), and to other metaloproteins (Sahlin et al., 1987; Styring and Rutherford, 1988; Innes and Brudvig, 1989; Hirsh et al., 1992a, b, 1993; Koulougliotis et al., 1995; Galli et al., 1995, 1996; Deligiannakis and Rutherford, 1996; Waldeck et al., 1997; Hung et al., 2000; Telser et al., 2000; Bar et al., 2001). The basic relation that has been used for the relaxation rate of the slow spin is:

$$(1/T_1) \approx \frac{|J|^2 S(S+1)\tau_{Fe}}{3(1+(\omega_{Fe}-\omega_{Cof})^2\tau_{Fe}^2)} \qquad (24)$$

where J is the magnitude of the spin-spin interaction, S the spin of the fast relaxer, and τ_{Fe} is the relaxation time of the metal ion. The Larmor frequency $\omega = g\mu_B H$ is well defined for free spins with $s = ½$, as in the case of the cofactors, ω_{Cof}. However, for a metal ion with $S \geq 1$, a free ion approximation is not valid for ω_{Fe} because it neglects the crystal field-splitting of the levels.

The main difference between Eq. 24 and Eq. 21 of the present spin dimer model arises from the neglect of the crystal field-splitting, Δ, of the transition metal ion. The phonons involved in the relaxation have an energy $\sim\Delta$, and not $(\omega_{Fe} - \omega_{Cof})$. Furthermore, the matrix elements of the interaction between the two spins are different. The neglect of the crystal field-splitting Δ in Eq. 24 can result in a large error of the derived value of $|J|^2$.

The inclusion of the crystal field-splitting is not only important for Fe^{2+} in bacterial photosynthetic reaction centers, but also in other systems in which it has been so far neglected, *e.g.*, the di-ferric spin-dimer appearing in ribonucleotide reductase (Sahlin et al., 1987; Hirsh et al., 1992b; Galli et al., 1995; Bar et al., 2001), the manganese cluster appearing in photosystem II (Styring and Rutherford, 1988; Innes and Brudvig, 1989; Hirsh et al., 1992a; Koulougliotis et al., 1995, 1997; Deligiannakis and Rutherford, 1996), and the Fe-S proteins (Waldeck et al., 1997; Hung et al., 2000; Telser et al., 2000). Even when the effects of the crystal field-splitting were observed in some of these cases, no detailed model was proposed to obtain a value of the spin-spin interaction from the relaxation data.

Multi-exponential time dependence of the relaxation rate

A multi-exponential time dependence of the relaxation rate may result from two causes: 1) if the magnetic interaction

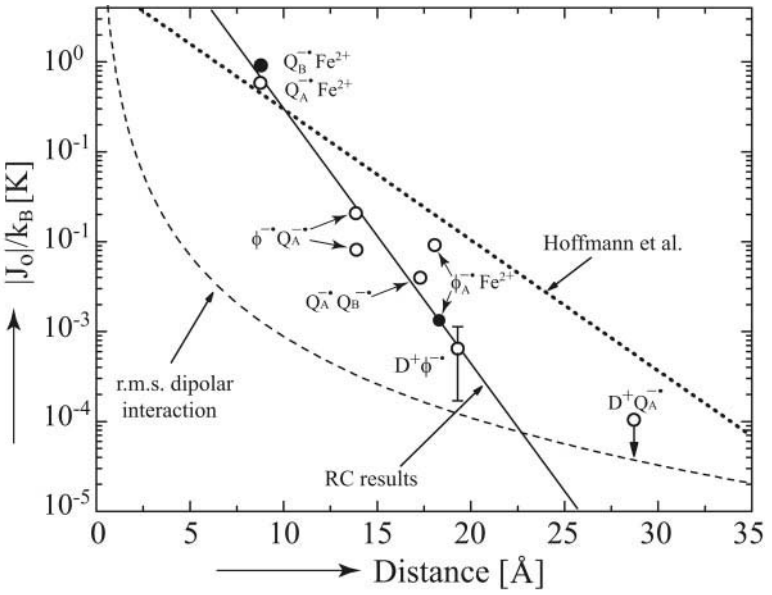

FIGURE 11 The exchange interaction between Fe^{2+} and cofactors and between cofactors in RCs (see Table 1). The results of this work are shown by ●, those of others by ○. The value for $D^+Q_A^-$ is an upper limit as indicated by the arrow. The dashed line is the root-mean-square magnitude of the dipolar contribution to the spin-spin interaction. The solid line is a fit to the RC data and the dotted line is an empirical relation proposed by Hoffmann et al. (1994) based mostly on data containing biradicals connected via σ-bonds.

between the spins is dipolar, the dependence of this interaction on the orientation of the magnetic field with respect to the molecular axes will result in a distribution of T_1 in a randomly oriented ensemble of molecules (frozen solution). 2) More than one excited state of the Fe^{2+} ion is involved in the relaxation process. This case is treated in Appendix B.

All of our data could be fitted well with a single exponential indicating that exchange interactions predominate over dipolar interactions. It also indicates that at the highest temperature of our experiments (4.2 K), essentially only the first excited Fe^{2+} level is populated. In contrast to our results Hirsch et al. (1992a, b, 1993) observed multi-exponential recoveries of the EPR signal, which they attribute to the predominance of dipolar interactions in their systems.

The magnitudes of J_y between the cofactors and the Fe^{2+} ion

The exchange interaction, J_o, is related to the electronic structure and the electron transfer rate between redox centers. A knowledge of its magnitude is, therefore, of prime importance. As mentioned in a previous section, the evaluation of A_M, and hence $|J_y|$, is difficult. We therefore resorted to a comparison of $|J_y|$ of $Q_B^-Fe^{2+}$ and ϕ^-Fe^{2+} with that of $Q_A^-Fe^{2+}$, which has been determined previously from a different set of measurements (Butler et al., 1980, 1984). This approach assumes that the other parameters (e.g., crystal field parameters D and E and elastic properties in the vicinity of the iron) remain constant.

From Eq. 20 we obtain:

$$J_y^2(\mathbf{Cof}) = \frac{A_M(\mathbf{Cof})}{A_M(Q_A^-)} J_y^2(Q_A^-) \qquad (25)$$

Using the values of A_M obtained from Fig. 10, *a* and *b* (Table 1) and the value of J_y between Q_A^- and Fe^{2+} (Butler et al., 1984), we calculated from Eq. 25 the values of $|J_y|$ between the other cofactors (Q_B^- and ϕ^-) and the Fe^{2+} ion (see Table 1). Note that A_M of $Q_B^-Fe^{2+}$ is ~3 times larger than A_M of $Q_A^-Fe^{2+}$ despite the Fe^{2+} ion being, within experimental error, equidistant from both quinones (see Table 1). A likely explanation is that the assumption of equal local phonon densities does not strictly hold. This is born out by a ~30% larger isotropic temperature factor (Debye-Waller or B-factor) obtained from the x-ray structure of Q_B^- compared to Q_A^- (Stowell et al., 1997; Abresch et al., 1999).

We assume that all interactions are antiferromagnetic ($J_y < 0$) and equal to the isotropic value ($J_o = J_y$), and plot the experimental values of $|J_o|$ in Fig. 11, as a function of the distance d between the spins. In Fig. 11 we include the magnitudes of the couplings between ϕ^- and Q_A^- (Okamura et al., 1979a, b; Van den Brink et al., 1996), between Q_A^- and Q_B^- (Calvo et al., 2000, 2001), between D^+ and ϕ^- (Moehl et al., 1985; Ogrodnik et al., 1987), and the upper limit for the exchange interaction between D^+ and Q_A^- (Zech et al., 1996).

The dipolar interaction between two cofactor spins with s = ½ is given by:

$$|J(\text{dipolar})|/k_B[\text{K}] = 0.3115\, g_{\text{Cof}_1} g_{\text{Cof}_2} d^{-3}[\text{Å}](1 - 3\cos^2\theta) \qquad (26)$$

where θ is the angle between the magnetic field and the axis joining the spins. Thus, from a sample with randomly oriented spin dimers one obtains a spread in J values. In Fig. 11 we plot the root-mean-square value of $|J(\text{dipolar})|/k_B$ (Eq. 26) between two spins with s = ½. The dipolar interaction between Fe^{2+} (S = 2) and a cofactor (s = ½) is ~4 times larger (not shown), depending on which Fe^{2+} states are involved. Fig. 11 shows that for distances smaller

than ~23 Å exchange interactions between the spins in the RC are larger than dipolar interactions. This explains the mono-exponential recovery of the EPR signal observed in this work. In contrast, the interaction between D^+ and Fe^{2+} ($d = 27$ Å, see Fig. 1) is expected to have a large dipolar component. This conclusion is supported by the results of Hirsh and Brudvig (1993), who observed multi-exponential recoveries of the signal from the primary donor D^+Fe^{2+} in RCs from *Rb. sphaeroides*, which they attributed to the anisotropy of the dipolar interaction (Eq. 26).

The exchange interaction, which involves the overlap of wavefunctions of the interacting species, is expected to depend exponentially on the distance, d, between them:

$$|J_o|/k_B \propto \exp(-\beta_J d) \tag{27}$$

The solid line in Fig. 11 represents the fit of the experimental data obtained on RCs (Table 1) with $\beta_J = 0.66$ Å^{-1}. This value is obtained when the distances are taken between the centers of the cofactor rings (Table 1 and Fig. 11). If the distances are taken between the closest points of the conjugate bonds of the cofactors, a value of $\beta_J = 0.86$ Å^{-1} is obtained (not shown). The dotted line represents the upper limit of the exchange interaction ($\beta_J = 0.33$ Å^{-1}) proposed by Hoffmann et al. (1994) using data obtained from a large number of compounds, including long biradicals in which the exchange interaction is transmitted through σ-bonds. These interactions are more effective than those transmitted through non-covalent and H-bonds or through space jumps, which explains the smaller β_J of 0.33 Å^{-1} obtained by Hoffmann et al. compared to 0.66-0.86 Å^{-1} in RCs.

The relation between electron transfer and exchange interaction between redox centers has been pointed out by several authors (Hopfield, 1974; Okamura et al., 1979a, b; DeVault, 1984; Hendrickson, 1985; Ogrodnik et al., 1987; Calvo et al., 2000). The result of a simple perturbation treatment of a two states model shows that the matrix element for electron transfer between states i and f, $|V_{if}|$, is related to the magnitude of the exchange coupling by (Okamura et al., 1979a, b; Calvo et al., 2000):

$$|V_{if}|^2 \approx U|J_o| \tag{28}$$

where U is the energy splitting between the ground and excited configurations.

Assuming that U is approximately constant for different redox centers, the distance dependence of $|J_o|$ (Eq. 27) and the electron transfer rate, which is proportional to $|V_{if}|^2$, should be the same. This is not found to be the case. For electron transfer β_{ET} was determined to be between 1.1 (Tezcan et al., 2001) and 1.4 Å^{-1} (Moser et al., 1992), whereas we find in this work a β_J of 0.66-0.86 Å^{-1}. The origin of this discrepancy is at present not understood. It may arise from the simplifying assumptions used in deriving Eq. 28, i.e., more than two states may need to be taken into account. This may be particularly important for the centers involving Fe^{2+}, which has six electrons in the open 3d shell. Also, the assumption that U is a constant for all centers may introduce an error that could make the distance dependence of $|V_{if}|^2$ different from that of J_o.

T_1 of radicals in other metalloproteins

In some proteins the fast relaxing species is not a single Fe^{2+} ion, but a dimer or cluster of magnetically coupled metal ions. These clusters have in general a group of low-lying excited states, as in the case of the Fe^{2+} ion, between which phonon-induced transitions occur. If a cofactor radical is magnetically coupled to that system, the two-step model described in this work may be used to study its spin-lattice relaxation. Such a system is the R2 subunit of ribonucleotide reductase, in which a tyrosine radical relaxes through the interaction with a diferric center (Sahlin et al., 1987; Hirsh et al., 1992b; Galli et al., 1995). Another system is photosystem(II), in which a cluster of manganese ions is coupled to the tyrosine radical Y_d (Styring and Rutherford, 1988; Innes and Brudvig, 1989; Hirsh et al., 1992a; Koulougliotis et al., 1995, 1997; Deligiannakis and Rutherford, 1996). In these systems the excited states play a crucial role in the relaxation processes of the cofactor spins. From the temperature dependence of the relaxation rate Galli et al. (1995) and Bar et al. (2001) showed the existence of excited states of the diferric center whose positions depend on the species from which the ribonuclease was obtained. However, these authors did not use an appropriate model for the relaxation of a radical interacting with a multi-state fast-relaxing center, which would have allowed them to calculate the interaction between the radical and the cluster. The spin dimer model (Eq. 17) presented in this work allows the calculation of the energies of the excited states of the fast-relaxing cluster, as well as the interaction between the cluster and the cofactor.

CONCLUSIONS

Interacting spins occur in many metalloproteins and other biomolecules. The interaction between the spins harbors information about the electronic and spatial structure of the complex. In this work we developed a theoretical model to determine the spin-spin interaction from the measured spin-lattice relaxation rate of a free radical coupled to a fast-relaxing metal ion (or cluster of ions). The model takes into account the zero field-splitting and the rhombicity of the metal ion, which play a crucial role in the relaxation process and which had been neglected in most previous treatments. The mechanism of spin-lattice relaxation of the spin dimer involves a two-phonon process, analogous to the one proposed by Orbach (1961) for rare earth ions.

The model was applied to the determination of the spin-spin interactions between Fe^{3+} and the cofactors bacteriopheophytin (ϕ^-) and quinones (Q_A^- and Q_B^-) in reaction centers from the photosynthetic bacterium *Rb. sphaeroides*.

For the three spin dimers ($\phi^{-}Fe^{2+}$, $Q_A^{-}Fe^{2+}$, and $Q_B^{-}Fe^{2+}$) we found that the exchange interaction $|J_o|$ dominates over the dipolar interaction.

The values of the exchange interactions between cofactors or between the Fe^{2+} and cofactors in bacterial photosynthetic reaction centers measured in this work and by other authors were plotted as a function of distance in Fig. 11. From these values a coefficient $\beta_J \sim (0.66\text{-}0.86)$ Å^{-1} was obtained for the exponential distance dependence of $|J_o|$ (see Eq. 27). This value is smaller than $\beta_{ET} \sim (1.1\text{-}1.4)$ Å^{-1}, proposed for the distance dependence of the electron transfer matrix elements $|V_{if}|^2$ (Moser et al., 1992; Tezcan et al., 2001). We ascribe the differences between β_J and β_{ET} to the simplifying assumptions used to derive Eq. 28, as explained in the text.

APPENDIX A

The transition rates k_{Fe}, k_{Cof}, and k_M

Expressions for the rates k_{Fe} and k_{Cof} can be derived from Van Vleck's spin-lattice relaxation theory (Van Vleck, 1940; Abragam and Bleaney, 1970; Orbach and Stapleton, 1972). The spin-lattice interactions $H_{sl}(\mathbf{S})$ and $H_{sl}(\mathbf{s})$ may be written as:

$$H_{Sl}(\mathbf{S}) = V(\mathbf{S})\varepsilon(\mathbf{r}_j), \quad H_{sl}(\mathbf{s}) = V(\mathbf{s})\varepsilon(\mathbf{r}_j)$$

where $V(\mathbf{S})$ and $V(\mathbf{s})$ are spin operators acting on the spins $\mathbf{S}$ and $\mathbf{s}$, and $\varepsilon(\mathbf{r}_j)$ is a time-varying deformation mode defined in terms of the positions $\mathbf{r}_j(t)$ of the ligands to the metal ion and cofactor. A sum of these products over different local modes of vibration needs to be considered in a detailed description. The transition rates between two spin states with the simultaneous emission ($k^{\downarrow}$) or absorption ($k^{\uparrow}$) of a phonon are given by:

$$k^{\uparrow} = An(\omega) \quad \text{and} \quad k^{\downarrow} = A[n(\omega) + 1] \qquad \text{(A1)}$$

where $n(\omega) = 1/(\exp(\hbar\omega/k_BT) - 1)$ is the phonon occupancy factor, i.e., the number of excitations for each mode with frequency ω. The constants A defined in Eq. A1 are (Abragam and Bleaney, 1970):

$$A_{Fe} = \frac{3\Delta^3}{2\pi\rho v^5\hbar}|\langle i|V(\mathbf{S})|j\rangle|^2, \quad A_{Cof} = \frac{3\delta^3}{2\pi\rho v^5\hbar}|\langle i|V(\mathbf{s})|j\rangle|^2 \qquad \text{(A2)}$$

where ρ is the local density of the material, v is the velocity of sound and $\langle i|V(\mathbf{S})|j\rangle$ and $\langle i|V(\mathbf{s})|j\rangle$ are the matrix element of $V(\mathbf{S})$ and $V(\mathbf{s})$ between the spin states of $\mathbf{S}$ and $\mathbf{s}$. The matrix elements of $V(\mathbf{s})$ are several orders of magnitude smaller than those of $V(\mathbf{S})$ because of the Kramers degeneracy of the spin states of the radical. The reason for the large matrix elements is the involvement of the orbitally degenerate states of the Fe^{2+} ion, whose energies are modulated by the fluctuating electric fields produced by the vibrations of the ligands. The value of the matrix elements of $V(\mathbf{S})$ for Fe^{2+} ions has been determined experimentally by EPR measurements performed under uniaxial stress (Watkins and Feher, 1962) and by ultrasonic absorption (Shiren, 1962, 1963) for Fe^{2+} impurities in MgO.

To calculate the transition rates k_M in Fig. 8 we consider the matrix elements of H_{sS} (Eq. 2) connecting the four energy states (Table IIB in Butler et al., 1984):

$$\langle 1\beta|H_{sS}|2\alpha\rangle = \langle 1\alpha|H_{sS}|2\beta\rangle = \frac{J_yP}{\sqrt{2}\Delta} \qquad \text{(A3)}$$

where

$$P = \frac{(1 + 3(E/D)^2)^{1/2} - 1 + 3(E/D)}{[((1 + 3(E/D)^2)^{1/2} - 1)^2 + 3(E/D)^2]^{1/2}} \qquad \text{(A4)}$$

depends on the rhombicity E/D of the Fe^{2+} ion. For Fe^{2+} in RCs, $E/D \approx 0.25$, and $P = 1.9$. The matrix elements (Eq. A3) mix the states $|1\alpha\rangle$, $|1\beta\rangle$, $|2\alpha\rangle$, $|2\beta\rangle$ allowing the spin-lattice interaction to produce transitions that change both $\mathbf{S}$ and $\mathbf{s}$. Due to these admixtures the matrix elements of $V(\mathbf{S})$ connecting the states having these admixtures (denoted by primes), $|1\alpha\rangle'$ with $|2\beta\rangle'$ and $|1\beta\rangle'$ with $|2\alpha\rangle'$, are:

$$\begin{aligned} {}'\langle 1\beta|V(\mathbf{S})|2\alpha\rangle' &= {}'\langle 1\alpha|V(\mathbf{S})|2\beta\rangle' \\ &= \frac{\langle 1\beta|H_{sS}|2\alpha\rangle/\Delta}{\langle 1|V(\mathbf{S})|1\rangle - \langle 2|V(\mathbf{S})|2\rangle} \\ &\approx \frac{J_yP}{\sqrt{2}\Delta}\langle 1\alpha|V(\mathbf{S})|2\beta\rangle \end{aligned} \qquad \text{(A5)}$$

When the Zeeman splitting δ is negligible compared with the zero field-splitting Δ, i.e., $\Delta \approx \Delta \pm \delta$, equal phonon densities are involved for the A_{Fe} and A_M processes, resulting in:

$$\frac{A_M}{A_{Fe}} = \left|\frac{\langle 1\alpha|V(\mathbf{S})|2\beta\rangle}{\langle 1\alpha|V(\mathbf{S})|2\alpha\rangle}\right|^2 \approx \frac{J_y^2P^2}{2\Delta^2} \qquad \text{(A6)}$$

In Eq. A6 J_y is the y component of the spin-spin interaction tensor defined in Eq. 2. Equations A5 and A6 assume that the principal directions of the $\mathbf{J}$ tensor and the zero field-splitting are the same. With this assumption the matrix elements giving rise to the transition rates labeled k_M in Fig. 8 depend only on the y component of the $\mathbf{J}$ tensor (Eq. 2), the y-direction being determined by the crystal field giving rise to the zero field-splitting (Eq. 3) (Butler et al., 1984).

To evaluate $k^{\downarrow}$ and $k^{\uparrow}$ one needs to know the parameters of the spin-lattice Hamiltonians ($H_{Sl}(\mathbf{S})$ and $H_{sl}(\mathbf{s})$ in Eq. 5) and the elastic properties of the medium (see Eqs. A1 and A2). This is a difficult task. Consequently, we use the ratio A_M/A_{Fe} (Eq. A6), which we assume to depend only on the properties of the Fe^{2+} ion and the component J_y of the spin-spin coupling.

APPENDIX B

Multi-exponential recovery of the populations in a multilevel spin system

Multi-exponential recoveries are expected for the populations N_i of a spin system having m levels. The system is described by m linear differential rate equations for the populations N_i of the levels ($i = 1, m$):

$$dN_i/dt = \sum_{j\neq i}(-k_{i\to j}N_i + k_{j\to i}N_j) = \sum_j W_{ij}N_j \qquad \text{(B7)}$$

The solution of Eq. B7 is:

$$N_i(t) = \sum_\gamma A_{i\gamma}\exp(-t/\tau_\gamma) \qquad \text{(B8)}$$

Where τ_γ are m relaxation times of the system obtained as eigenvalues of the $m \times m$ matrix W_{ij} defined in Eq. B7. The coefficients $A_{i\gamma}$ in Eq. B8

depend on the initial values $N_i(t = 0)$ for the populations, and thus on experimental conditions. Because $\sum_i N_i = N$ is a constant, the rate matrix W_{ij} defined in Eq. B7 is degenerate and one rate $1/\tau_\gamma = 0$ in Eq. B8. This sets the Boltzmann condition as the equilibrium condition for the populations for $t \rightarrow \infty$ at a non-saturating microwave power. The approach to this equilibrium is reached through $(m - 1)$ relaxation times. As shown by McCumber (1963), Eq. B7 provides an alternate way to consider the relaxation mechanism through excited states proposed by Orbach (1961). Under the special conditions invoked in Eqs. 10 and 14 to obtain Eqs. 16 and 17, a four-level spin system has a single relaxation time. At temperatures higher than ~10 K the populations of the higher excited levels of the Fe^{2+} ion of the photosynthetic RC in Fig. 7 are important, which makes it necessary to use Eq. B7 in the analysis of the relaxation of the cofactors. In this case a multi-exponential recovery of the populations is expected.

We thank Herb Axelrod and Mark Paddock for helpful discussions and Clemens Krucken for the development of software used for data acquisition.

This work was supported by grants from the National Institute of Health NIH (GM 13191) and National Science Foundation (MCB 99-82186).

REFERENCES

Abragam, A. 1955. Overhauser effect in nonmetals. *Phys. Rev*. 98: 1729–1735.

Abragam, A. 1961. The Principles of Nuclear Magnetism. Clarendon Press, Oxford.

Abragam, A., and B. Bleaney. 1970. Electron Paramagnetic Resonance of Transition Ions. Clarendon Press, Oxford.

Abresch, E. C., A. P. Yeh, S. M. Soltis, D. C. Rees, H. L. Axelrod, M. Y. Okamura, and G. Feher. 1999. Crystal structure of the charge separated state $D^+Q_A^-$ in photosynthetic reaction centers from *Rb. sphaeroides*. *Biophys. J.* 76:141*a*. (Abstr.).

Allen, J. P., G. Feher, T. O. Yeates, H. Komiya, and D. C. Rees. 1987a. Structure of the reaction center from *Rhodobacter sphaeroides* R-26.I. The cofactors. *Proc. Natl. Acad. Sci. USA.* 84:5730–5734.

Allen, J. P., G. Feher, T. O. Yeates, H. Komiya, and D. C. Rees. 1987b. Structure of the reaction center from *Rhodobacter sphaeroides* R-26.II. The protein subunits. *Proc. Natl. Acad. Sci. USA.* 84:6162–6166.

Allen, J. P., G. Feher, T. O. Yeates, H. Komiya, and D. C. Rees. 1988. Structure of the reaction center from *Rhodobacter sphaeroides* R-26: Protein-cofactor (quinones and Fe^{2+}) interactions. *Proc. Natl. Acad. Sci. USA.* 85:8487–8491.

Allen, J. P., G. Feher, T. O. Yeates, D. C. Rees, J. Deisenhofer, H. Michel, and R. Huber. 1986. Structural homology of reaction centers from *R. sphaeroides* and *R. viridis* as determined by x-ray diffraction. *Proc. Natl. Acad. Sci. USA.* 83:8589–8593.

Anderson, P. W. 1959. New approach to the theory of superexchange interactions. *Phys. Rev.* 115:2–13.

Bar, G., M. Bennati, H. T. Nguyen, J. Ge, J. Stubbe, and R. G. Griffin. 2001. High-frequency (140 GHz) time domain EPR and ENDOR spectroscopy. The tyrosyl radical-diiron cofactor in ribonucleotide reductase from yeast. *J. Am. Chem. Soc.* 123:3569–3576.

Bencini, A., and D. Gatteschi. 1990. Electron Paramagnetic Resonance of Exchange Coupled Systems. Springer-Verlag, Berlin.

Bloembergen, N. 1949. On the interaction of nuclear spins in a crystalline lattice. *Physica.* 15:386–426.

Bloembergen, N., and L. O. Morgan. 1961. Proton relaxation times in paramagnetic solutions. Effect of electron spin relaxation. *J. Chem. Phys.* 34:842–850.

Bloembergen, N., E. M. Purcell, and R. V. Pound. 1948. Relaxation effects in nuclear magnetic resonance absorption. *Phys. Rev.* 73:679–712.

Bowman, M. K., J. R. Norris, and C. A. Wraight. 1979. Distance determination in bacterial photoreaction centers by electron spin relaxation. *Biophys. J.* 25:203*a*. (Abstr.).

Butler, W. F., R. Calvo, D. R. Fredkin, R. A. Isaacson, M. Y. Okamura, and G. Feher. 1984. The electronic structure of Fe^{2+} in reaction centers from *Rhodopseudomonas sphaeroides*. III. EPR measurements of the reduced acceptor complex. *Biophys. J.* 45:947–973.

Butler, W. F., D. C. Johnston, H. B. Shore, D. R. Fredkin, M. Y. Okamura, and G. Feher. 1980. The electronic structure of Fe^{2+} in reaction centers from *Rhodopseudomonas sphaeroides*. I. Static magnetization measurements. *Biophys. J.* 32:967–992.

Calvo, R., E. C. Abresch, R. Bittl, G. Feher, W. Hofbauer, R. A. Isaacson, W. Lubitz, M. Y. Okamura, and M. L. Paddock. 2000. EPR study of the molecular and electronic structure of the semiquinone biradical $Q_A^-Q_B^-$ in photosynthetic reaction centers from *Rhodobacter sphaeroides*. *J. Am. Chem. Soc.* 122:7327–7341.

Calvo, R., W. F. Butler, R. A. Isaacson, M. Y. Okamura, D. R. Fredkin, and G. Feher. 1982. Spin-lattice relaxation time of the reduced primary quinone in RCs from *R. sphaeroides*: determination of the zero field splitting of Fe^{2+}. *Biophys. J.* 37:111*a*. (Abstr.).

Calvo, R., R. A. Isaacson, E. C. Abresch, M. Y. Okamura, and G. Feher. 1999. Spin-lattice relaxation of ϕ^- in bacterial photosynthetic reaction centers. *Biophys. J.* 76:357a. (Abstr.).

Calvo, R., R. A. Isaacson, M. L. Paddock, E. C. Abresch, M. Y. Okamura, A. L. Maniero, L. C. Brunel, and G. Feher. 2001. EPR study of the semiquinone biradical $Q_A^-Q_B^-$ in photosynthetic reaction centers of *Rb. sphaeroides* at 326 GHz. Determination of the exchange interaction J_o. *J. Phys. Chem. B.* 105:4053–4057.

Chang, C. H., D. Tiede, J. Tang, U. Smith, J. R. Norris, and M. Schiffer. 1986. Structure of *Rhodopseudomonas-Sphaeroides* R26 reaction center. *FEBS Lett.* 205:82–86.

Coffman, R. E., and G. R. Buettner. 1979. A limit function for long-range ferromagnetic and antiferromagnetic superexchange. *J. Phys. Chem.* 83:2387–2392.

Cramer, W. A., and D. B. Knaff. 1991. Energy transduction in biological membranes. Springer, New York.

Debus, R. J., G. Feher, and M. Y. Okamura. 1986. Iron-depleted reaction centers from *Rhodopseudomonas sphaeroides* R-26.1: characterization and reconstitution with Fe^{2+}, Mn^{2+}, Co^{2+}, Ni^{2+}, Cu^{2+}, Zn^{2+}. *Biochemistry.* 25:2276–2287.

Deisenhofer, J., O. Epp, I. Sinning, and H. Michel. 1995. Crystallographic refinement at 2.3-Å resolution and refined model of the photosynthetic reaction-center from *Rhodopseudomonas-viridis*. *J. Mol. Biol.* 246: 429–457.

Deligiannakis, Y., and A. W. Rutherford. 1996. Spin-lattice relaxation of the pheophytin, $Pheo^-$, radical of photosystem II. *Biochemistry.* 35: 11239–11246.

DeVault, D. 1984. Quantum mechanical tunneling in biological systems. Cambridge University Press, London.

Ermler, U., G. Fritzsch, S. K. Buchanan, and H. Michel. 1994. Structure of the photosynthetic reaction center from *Rhodobacter sphaeroides* at 2.65 Å resolution: cofactors and protein cofactor interactions. *Structure.* 2:925–936.

Feher, G. 1957. Sensitivity considerations in microwave paramagnetic resonance absorption techniques. *Bell Syst. Tech. J.* 36:449–484.

Feher, G. 1992. Identification and characterization of the primary donor in bacterial photosynthesis: a chronological account of an EPR-ENDOR investigation. *J. Chem. Soc. Perkin Trans.* 2:1861–1874.

Feher, G., and M. Y. Okamura. 1999. The primary and secondary acceptors in bacterial photosynthesis. II. The structure of the Fe^{2+}-Q^- complex. *Appl. Magn. Reson.* 16:63–100.

Galli, C., M. Atta, K. K. Andersson, A. Gräslund, and G. W. Brudvig. 1995. Variations of the diferric exchange coupling in the R2 subunit of ribonucleotide reductase from four species as determined by saturation-recovery EPR spectroscopy. *J. Am. Chem. Soc.* 117: 740–746.

Galli, C., R. MacArthur, H. M. Abu-Soud, P. Clark, D. J. Stuehr, and G. W. Brudvig. 1996. EPR spectroscopic characterization of neuronal NO synthase. *Biochemistry.* 35:2804–2810.

Hendrickson, D. N. 1985. Magnetic exchange interactions propagated by multi-atom bridges. *In* Magneto-Structural Correlations in Exchange

Coupled Systems. R. D. Willet, D. Gatteschi, and O. Kahn, editors. Reidel, Dordrecht. 523–554.

Herrick, R. C., and H. J. Stapleton. 1976. Determination of the zero field splitting of Fe^{3+} in cytochrome P-450 from electron spin-lattice relaxation times. *J. Chem. Phys.* 65:4786–4790.

Hirsh, D. J., W. F. Beck, J. B. Innes, and G. W. Brudvig. 1992a. Using saturation-recovery EPR to measure distances in proteins: applications to photosystem II. *Biochemistry.* 31:532–541.

Hirsh, D. J., W. F. Beck, J. B. Lynch, L. Que, Jr., and G. W. Brudvig. 1992b. Using saturation-recovery EPR to measure exchange couplings in proteins: application to ribonucleotide reductase. *J. Am. Chem. Soc.* 114:7475–7481.

Hirsh, D. J., and G. W. Brudvig. 1993. Long-range electron spin-spin interactions in the bacterial photosynthetic reaction center. *J. Phys. Chem.* 97:13216–13222.

Hoffmann, S. K., W. Hilczer, and J. Goslar. 1994. Weak long-distance superexchange interaction and its temperature variations in copper(II) compounds studied by single crystal EPR. *Appl. Magn. Res.* 7:289–321.

Hopfield, J. J. 1974. Electron transfer between biological molecules by thermally activated tunneling. *Proc. Natl. Acad. Sci. USA.* 71: 3640–3644.

Hung, S. C., C. V. Grant, J. M. Peloquin, A. R. Waldeck, R. D. Britt, and S. L. Chan. 2000. Electron spin-lattice relaxation measurement of the 3Fe-4S (S-3) cluster in succinate:ubiquinone reductase from *Paracoccus denitrificans*. A detailed analysis based on a dipole-dipole interaction model. *J. Phys. Chem. A.* 104:4402–4412.

Hyde, J. S., H. M. Swartz, and W. E. Antholine. 1979. The spin-probe-spin-label method. *In* Spin Labeling II: Theory and Applications. L. J. Berliner, editor. Academic Press, New York. 71–113.

Innes, J. B., and G. W. Brudvig. 1989. Location and magnetic relaxation properties of the stable tyrosine radical in photosystem II. *Biochemistry.* 28:1116–1125.

Isaacson, R. 1968. Use of field modulation with boxcar integrator to measure relaxation time in electron spin resonance. *J. Sci. Instrum.* 1:1137–1139.

Isaacson, R. A., F. Lendzian, E. C. Abresch, W. Lubitz, and G. Feher. 1995. Electronic structure of Q_A^- in reaction centers from *Rhodobacter sphaeroides*. I. Electron paramagnetic resonance in single crystals. *Biophys. J.* 69:311–322.

Kahn, O. 1993. Molecular Magnetism. VCH, New York.

Kittel, C. 1996. Introduction to Solid State Physics, 7th ed. Wiley, New York.

Koulougliotis, D., R. H. Schweitzer, and G. W. Brudvig. 1997. The tetranuclear manganese cluster in photosystem II: location and magnetic properties of the S2 state as determined by saturation-recovery EPR spectroscopy. *Biochemistry.* 36:9735–9746.

Koulougliotis, D., X. S. Tang, B. A. Diner, and G. W. Brudvig. 1995. Spectroscopic evidence for the symmetric location of tyrosines D and Z in photosystem II. *Biochemistry.* 34:2850–2856.

Kulikov, A. V., and G. I. Likhtenstein. 1977. The use of spin relaxation phenomena in the investigation of the structure of model and biological systems by the method of spin labels. *Adv. Molec. Relax. Interac. Processes.* 10:47–79.

Lakshmi, K. V., and G. W. Brudvig. 2000. Electron paramagnetic resonance distance measurements in photosystems. *In* Biological Magnetic Resonance, Vol. 19, Chap. 12. L. J. Berliner, G. R. Eaton, S. S. Eaton, editors. Kluwer Academic/Plenum, New York. 513–567.

Lubitz, W., and G. Feher. 1999. The primary and secondary acceptors in bacterial photosynthesis. III. Characterization of the quinone radicals Q_A^- and Q_B^- using EPR and ENDOR. *Appl. Magn. Reson.* 17:1–48.

McCumber, D. E. 1963. Comments on spin-lattice relaxation. *Phys. Rev.* 130:2271–2276.

McElroy, J. D., D. C. Mauzerall, and G. Feher. 1974. Characterization of primary reactants in bacterial photosynthesis II. Kinetic studies of the light-induced signal ($g = 2.0026$) and the optical absorbance changes at cryogenic temperatures. *Biochim. Biophys. Acta.* 333: 261–278.

Michel-Beyerle, M. E., M. Bixon, and J. Jortner. 1988. Interrelation between primary electron transfer dynamics and magnetic interactions in photosynthetic reaction centers. *Chem. Phys. Lett.* 151:188–194.

Moehl, K. W., E. J. Lous, and A. J. Hoff. 1985. Low-power, low-field RYDMAR of the primary radical pair. *Chem. Phys. Lett.* 121:22–27.

Moriya, T. 1960. Anisotropic superexchange interaction and weak ferromagnetism. *Phys. Rev.* 120:91–98.

Moser, C. C., J. M. Keske, K. Warncke, R. S. Farid, and P. L. Dutton. 1992. Nature of biological electron transfer. *Nature.* 355:796–802.

Norris, J. R., M. C. Thurnauer, and M. K. Bowman. 1980. Electron spin echo spectroscopy and the study of biological structure and function. *Adv. Biol. Med. Phys.* 17:365–416.

Ogrodnik, A., N. Remy-Richter, M. E. Michel-Beyerle, and R. Feick. 1987. Observation of activationless recombination in reaction centers of *R. sphaeroides*. A new key to the primary electron-transfer mechanism. *Chem. Phys. Lett.* 135:576–581.

Okamura, M. Y., D. R. Fredkin, R. A. Isaacson, and G. Feher. 1979a. Magnetic interactions and electron transfer kinetics of the reduced intermediate acceptor in reaction centers (RCs) of *Rhodopseudomonas sphaeroides* R-26. Evidence for thermally induced tunneling. *In* Tunneling in Biological Systems. B. Chance, D. C. DeVault, H. Frauenfelder, R. A. Marcus, J. R. Schriefer, and N. Sutin, editors. Academic Press, New York. 729–743.

Okamura, M. Y., R. A. Isaacson, and G. Feher. 1979b. Spectroscopic and kinetic properties of the transient intermediate acceptor in reaction centers from *Rhodopseudomonas sphaeroides*. *Biochim. Biophys. Acta.* 546:394–417.

Orbach, R. 1961. Spin-lattice relaxation in rare-earth salts. *Proc. R. Soc. A (Lond.).* 264:458–484.

Orbach, R., and H. J. Stapleton. 1972. Electron spin-lattice relaxation. *In* Electron Paramagnetic Resonance. S. Geschwind, editor. Plenum, New York.

Sahlin, M., L. Peterson, A. Gräslund, A. Ehrenberg, B. M. Sjöberg, and L. Thelander. 1987. Magnetic interaction between the tyrosyl free radical and the antiferromagnetically coupled iron center in ribonucleotide reductase. *Biochemistry.* 26:5541–5548.

Scholes, C. P., R. A. Isaacson, and G. Feher. 1971. Determination of the zero field splitting of Fe^{3+} in heme proteins from the temperature dependence of the spin-lattice relaxation rate. *Biochim. Biophys. Acta.* 244:206–210.

Shiren, N. S. 1962. Spin phonon interactions for Cr^{3+}, Mn^{2+}, Fe^{3+}, Fe^{2+} and Ni^{2+} in MgO. *Bull. Am. Phys. Soc.* 7:29.

Shiren, N. S. 1963. Comparison of ultrasonic spin resonance measurements with paramagnetic resonance theory. *In* Magnetic and Electric Resonance and Relaxation. J. Smidt, editor. North Holland, Amsterdam. 114–122.

Slichter, C. P. 1990. Principles of Magnetic Resonance. Springer, Berlin.

Stowell, M. H. B., T. M. McPhillips, D. C. Rees, S. M. Soltis, E. Abresch, and G. Feher. 1997. Light-induced structural changes in the photosynthetic reaction center: implications for the mechanism of electron/proton transfer. *Science.* 276:812–816.

Styring, S. A., and A. W. Rutherford. 1988. The microwave power saturation of SII_{slow} varies with the redox state of the oxygen evolving complex in photosystem II. *Biochemistry.* 27:4915–4923.

Telser, J., H. Lee, and B. M. Hoffman. 2000. Investigation of exchange couplings in $[Fe_3S_4]^+$ clusters by electron spin-lattice relaxation. *J. Biol. Inorg. Chem.* 5:369–380.

Tezcan, F. A., B. R. Crane, J. R. Winkler, and H. B. Gray. 2001. Electron tunneling in protein crystals. *Proc. Natl. Acad. Sci. USA.* 98:5002–5006.

Utschig, L. M., S. R. Greenfield, J. Tang, P. D. Laible, and M. C. Thurnauer. 1997. Influence of iron-removal procedures on sequential electron transfer in photosynthetic bacterial reaction centers studied by transient EPR spectroscopy. *Biochemistry.* 36:8548–8558.

Van den Brink, J. S., P. Gast, and A. J. Hoff. 1996. Magnetic interactions between the reduced bacteriopheophytin and quinone electron acceptors in reaction centers of the purple bacterium *Rhodopseudomonas viridis*:

an X-band and Q-band electron paramagnetic resonance study. *J. Chem. Phys.* 104:1805–1812.

Van Vleck, J. H. 1940. Paramagnetic relaxation times for titanium and chrome alum. *Phys. Rev.* 57:426–448.

Waldeck, A. R., M. H. B. Stowell, H. K. Lee, S.-C. Hung, M. Matsson, L. Hederstedt, B. A. C. Ackrell, and S. I. Chan. 1997. Electron paramagnetic resonance studies of succinate:ubiquinone oxidoreductase from *Paracoccus denitrificans*. *J. Biol. Chem.* 272: 19373–19382.

Watkins, G. D., and E. Feher. 1962. Effect of uniaxial stress on the EPR of transition metal ions. *Bull. Am. Phys. Soc.* 7:29.

Yeates, T. O., H. Komiya, A. Chirino, D. C. Rees, J. P. Allen, and G. Feher. 1988. Structure of the reaction center from *Rhodobacter sphaeroides* R-26: protein-cofactor (quinones and Fe^{2+}) interactions. *Proc. Natl. Acad. Sci. USA.* 85:7993–7997.

Yeates, T. O., H. Komiya, D. C. Rees, J. P. Allen, and G. Feher. 1987. Structure of the reaction center from *Rhodobacter sphaeroides* R-26: membrane-protein interactions. *Proc. Natl. Acad. Sci. USA.* 84: 6438–6442.

Zech, S. G., W. Lubitz, and R. Bittl. 1996. Pulsed EPR experiments on radical pairs in photosynthesis: comparison of the donor acceptor distances in photosystem I and bacterial reaction centers. *Ber. Bunsenges. Phys. Chem.* 100:2041–2044.